UNIVERSITÀ
DEGLI STUDI
DI PADOVA


**Dipartimento di Ingegneria Industriale DII**

**Corso di Laurea Magistrale in Ingegneria Meccanica**


# ANALYTICAL AND NUMERICAL MODELLING OF SELF-HEATING PHENOMENA DUE TO DAMAGE IN COMPOSITE STRUCTURES


**Relatori:**

**Prof. Marie-Laetitia Pastor**

**Prof. Mauro Ricotta**

**Presentata da:**

**Nicolò Zacchettin**

**Matricola 1185151**



**Anno Accademico 2020/2021**

# Abstract

This work is intended to investigate analytically and numerically the correlation between self-heating phenomena and damage in CFRP composites subjected to cyclic loading. The aim of this work is to elaborate a model that takes into account the material degradation in order to quantify damage evolution. To accomplish this result a new model, based on two previous theories, is set. The idea is to separate and quantify the heat generation sources that are involved during a fatigue test. This new model, integrating Representative Volume Element simulations, analyses the microstructural behavior of the laminate on the commercial software Abaqus. Numerical results are then compared to data obtained with a different process, in order to validate the model.

**Keywords:** Self-heating, Fatigue, Representative Volume Element, Damage, CFRP laminates

# Contents

# List of Figures

# 1 Introduction

Composite materials and precisely Carbon Fibre Reinforced Polymer (CFRP) are widely used because of their high specific strength, high rigidity and good corrosion resistance. Their performances outweigh the metals and in many different fields structures are now realized in composite materials instead of steel. However, despite multiple benefits, CFRP structures hide some weaknesses. The fatigue behavior of composites depends on way more factors than that of metals. For example the stacking sequence, the volume fraction, manufacturing process, etc. Composites because of their heterogeneous composition, present degradation mechanisms that are complex and not easy to uncouple. A difficulty in understanding damage nature makes the prediction of fatigue behavior harder.

However, recent techniques based on infrared thermography (IRT) are capable of determining the fatigue limit very quickly. By pointing an infrared camera to a specimen subjected to cyclic loading, temperature evolution is recorded. This measurement allows thermo-mechanical considerations that can correlate fatigue limit and temperature. The objective, which often is finding the fatigue limit and predict the $S-N$ curve can be reached even if the reasons behind temperature variation of CFRP are not described accurately.

This work has the purpose of making a step towards the comprehension of the correlation of damage evolution and self-heating in CFRP. The idea is to quantify and distinguish the energies that are generated and dissipated through a cyclic loading test. These values can be a reference for future observation of material degradation in order to build a material model able to describe the complex behavior of composites.

For this purpose, a new model is developed. It describes temperature variation as the sum of different terms. Then a micro-scale numerical model, based on Represen-

tative Volume Elements, is used to investigate the behavior of fibre and matrix. In conclusion, results are compared with previous studies on the same problem in order to validate the new proposed model.

# 2 Background

This work is focused on CFRP composites. A deep knowledge of their composition and behavior is essential to understand the phenomena that occur during their life. Also, the relation between damage evolution and self-heating is based on many different thermodynamic considerations.

## 2.1 Carbon Fibre Reinforced Polymer Composites

Composite materials are made of at least two phases combined at microscopic level. These constituent materials are merged to achieve improved and better properties compared to those of the individual elements [5]. Usually one component is a continuous matrix phase and another is a reinforcing phase. The matrix materials can be polymers, metals and ceramics. Reinforcement materials can be fibres (long or short), spheres, particles or else.

Composites are created to absolve needs of the designer in order to obtain extremely performing materials in a precise sector. Most studied properties are for example: density, Young's modulus, strength, specific heat, thermal expansion coefficient, thermal conductivity, thermal diffusivity, dielectric constant and electric conductivity.

One of the most commonly used composite material is Carbon Fibre Reinforced Polymer (CFRP) which is peculiar for its high stiffness, high strength-to-weight ratio, high fatigue life. Figure 1 shows an ideal structure of unidirectional CFRP.

The matrices of CFRP are thermosetting or thermoplastic polymers. Reinforcements fibres can be long, short or a mix and they can be oriented, random or woven. The mechanical properties of CFRP composite are determined by those constituents and their disposition. The matrix gives consistency to the composite, holding fibres together in the designed shape, but mainly it provides distribution of tensions among fibres and protects from environmental attacks. A good matrix has excellent adhesion, good plasticity, high resistance to corrosion. The fibres, on the other hand, carry the majority of

Figure 1: Structure of Carbon Fibre Reinforced Polymer (CFRP) [20]

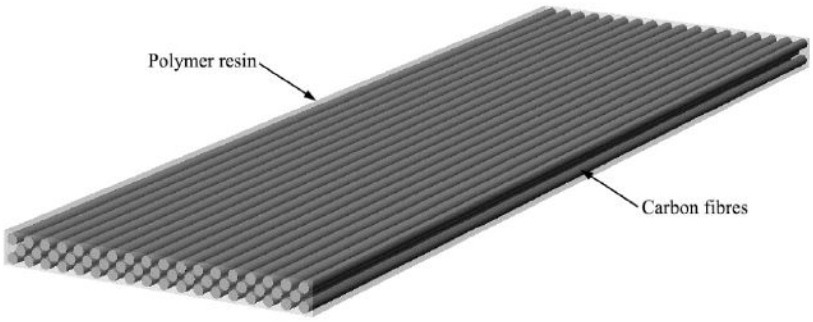


the load and contribute with most of the stiffness and strength. Composite materials are commonly used as laminates, a sequence of tight layers made of matrix and fiber [19] . In this work are only considered laminates which layers are unidirectional plies. This kind of fabric consists of plans of parallel fibres, oriented on a single direction. In order to keep fibres in position and to make manipulation easier, a very light seam is operated or some transverse fibres are woven. This setup allows to place fibres along precise directions even on big dimensions components.[6] [20]

### 2.1.1 Carbon Fibres

Carbon fibres achieve the best mechanic performance. They can reach extremely high values keeping density values comparable to aramid and glass fibres. The production process establishes a strongly anisotropic disposition of chains, so that excellent traction properties are obtained. Strong bonds operate mostly in this direction while Van der Waals bonds lead to poor shear resistance. On the same principles, carbon fibres do not perform well under compression where values are way lower than in traction.
For example they can be divided by their Young's modulus in: SM *standard modulus*, IM *Intermediate modulus*, HM *high modulus* and UHM *ultra high modulus*. At the same time they are divided by their tensile strength. The most common reinforcements are HS *high strength* and IM *intermediate modulus*.
Given their high cost -a carbon fibre reinforcement costs 5 times a glass fibres one -

CFRP is used partially in nautical applications where dimensions are relevant and it is widely used in the aerospace industry where budgets are higher and weight makes the difference.

### 2.1.2 Epoxy resin

Thermosetting matrices belong to different polymers families that share the ability of hardening by creating chemical bonds between chains during polymerization. This process is called cross-linking and lets the polymer create a very strong net. Mechanical properties of these resins mainly depend on the molecular units of which are composed, on the length of the chains and on the disposition of transverse cross-links. Polymerization can occur at ambient temperature, this make them suitable for crafting components of large dimensions. Some resins need heating to complete polymerization, that is why some further processes, known as post-curing, take place. Generally speaking, these polymers' behaviour is brittle and isotropic. Differently from thermoplastic polymers they can't be re-processed by heating up.

In particular, epoxy resin has better mechanical properties and less toxicity than the other thermosetting resins. The resin considered in this work, EPL 1012 is realized by using Bisphenol F linked to amines. Its low viscosity allows for complete impregnation of reinforcement fibres of carbon.

## 2.2 Failure and damage

In the vast majority of structural applications, the most stressed components, and therefore also composite components, are subjected to time-varying loads that can induce fatigue damage. This results in a loss of stiffness, first, and then component failure. It is therefore clear the importance of properly considering the phenomenon of fatigue when designing a composite component.Thermograpghic analyses on composites

are an effective solution to monitor damage evolution and to give designers the right tools. In considering how the damage is triggered and evolves in a composite structure, it is important to highlight how fatigue design can be approached more broadly than simply calculating the number of cycles at break. The possible approaches are in fact the following:

i Trigger design

ii Stiffness design

iii Resistance design

From a conservative, but also functional point of view, the first approach (i) is aimed at avoiding the initiation of any form of damage. This may be the case of particularly critical components such as primary structural elements in the automotive and aeronautical sectors or pressure vessels, where the presence of a crack leads to fluid leakage. On the other hand, the other two approaches are part of a damage tolerant design approach, in which the presence of damage can be accepted, provided that it is not such as to cause a decrease in stiffness beyond a certain threshold (ii) or such as to compromise the ability to withstand the operating load (iii)[15].

Many authors classify the numerous failure modes of composite materials in four main categories of damage:

- fibre breaking in traction or compression
- progressive damage of matrix (transverse matrix cracking)
- damage of fibre-matrix interface (interfacial debonding)
- delamination phenomena

Fibre breakage is a brittle damage, it usually occurs when the load is aligned with the reinforce direction. It is a probabilistic phenomenon, the strength of fibres is distributed with a certain probability distribution inside the reinforcement layers. In

addition, failure of isolated groups of fibres does not imply separation because load can be transferred to other fibres. The object of the study are long fibres reinforcement (fiber length > critic length), according to this, failure of the material happens due to fibre breakage. For the same reason, pull-out phenomenon is neglected. Matrix and evolution of damage in it play an important role for two reasons:

- Areas where matrix is damaged represent areas of over-stress for the fibres
- Matrix has the function of load transfer and when fibre-matrix interface fracture occurs, that action is compromised.

Failure occurs when fibres adjacent to the interrupted ones can no more withstand over-stress.

Matrix micro-cracking can be easily detected in multi-layer laminates with $[0, 90]_{ns}$ plies, as it is presented in Figure 2. On the other hand, Figure 3 shows a crack's path through the matrix. The matrix of the layers non-oriented with the load is exposed to a micro-cracking process due to the stress originated by respecting the congruence condition of the laminate. The peculiarity of this damage condition is that it comes to a saturation in the layers stressed crosswise. Indeed, despite cracking, interlaminar interface is still loaded thanks to the shear flow given by the adjacent layers. Once cracks density outcomes a critical value, distance between cracks is no more enough to allow other fractures to generate. This phenomenon only reduces mechanical properties in matrix-dominated directions, so along the reinforcement direction its effect is negligible. This damage mechanism is not the only that can lead to interlaminar cracks in the matrix. It is possible that some cracks oriented with the load direction appear. The formation of this kind of fractures, typical of the unidirectional reinforcement, is connected to the different Poisson coefficient of layers oriented in load direction and the those in transverse direction. Layers at 0° tend to a contraction, but this behavior is prevented by the stiffness of 90° layers. This way, the $\sigma_{yy}$ that originates can lead to the formation of matrix cracks parallel to the fibres. However, this damage mode

is less relevant than transverse matrix cracking considering the entire damage of the laminate.

Figure 2: Damage on a cross-ply laminate [14]

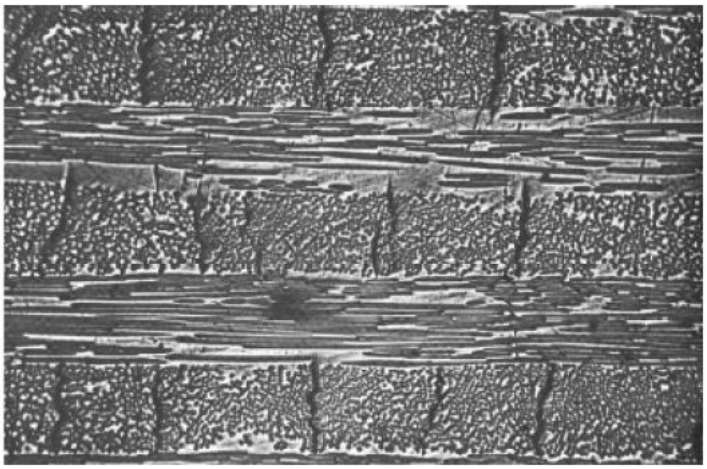

Figure 3: Transverse crack through the matrix [14]

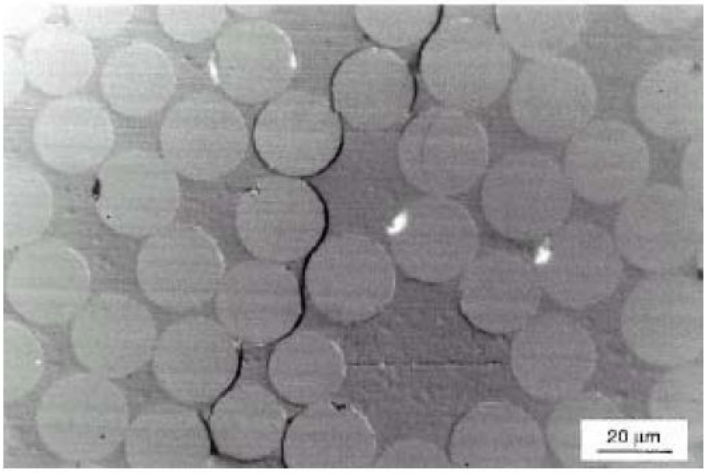


Debonding is the disconnection between fiber and matrix and it occurs when damage involves their interface. Such failure mode is typically brittle.

Delamination consists in physical detachment of two layers. It happens after impacts, indentations or it is due to interlaminar peeling stress, acting outside the laminate

plan. Generally it is a result of other damage modes, matrix micro cracking in particular which can be the trigger for interlaminar fracture. Figure 4 shows how transverse cracking turned into delamination. [14]

Figure 4: Delamination in presence of transverse matrix cracking [14]

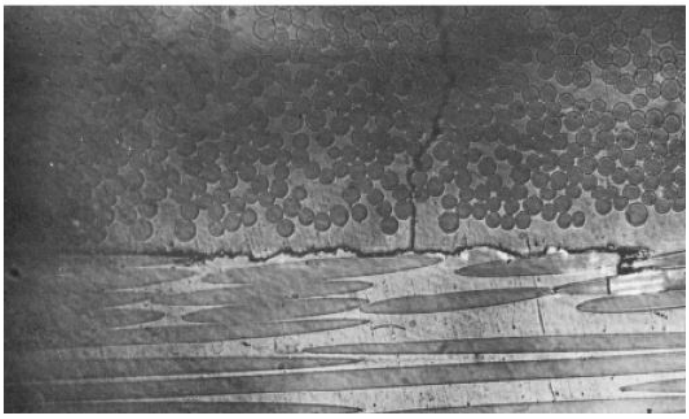

### 2.2.1 Fatigue damage

The evolution of fatigue damage in composite laminates with unidirectional reinforcement is a complex phenomenon, characterized by different mechanisms that follow and interact.

i Matrix cracking. In the early stages of life, the first mechanism of damage observable at macroscopic level is the initiation of cracks in the most disadvantaged oriented layers compared to external loads (off-axis cracks). Imagining a simple multidirectional specimen subject to a mono-axis external load, with a state of uniform stress in the laminate plane, the position of the trigger points of the first cracks is purely stochastic, determined by the presence of defects or inhomogeneities in the microstructure. The number of cycles spent for the initiation of the first cracks, on the other hand, depends on the tensional level to which the off-axis layer is subjected. It is widely proven that there is a power relationship (Wohler type) between the maximum cycle stress level and the number of cycles to

the trigger. Figure 5 shows initiation and early propagation of an off-axis matrix crack.

Figure 5: Damage on microscopic scale: a) off-axis crack initiation and b) propagation [15]

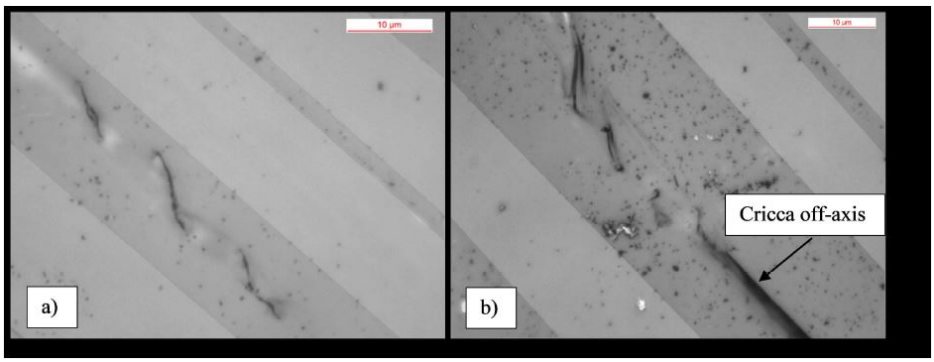


ii Delamination. the number of cycles increases, previous cracks propagate, as well as new cracks are generated, up to a state of saturation. In this phase the laminate, although still able to withstand the load, may have lost a significant part of its initial stiffness, due to the presence of off-axis cracks. In correlation to the saturation of the transverse cracks, delaminations are induced and begin to propagate at the interface between the layers, which originate at the apexes of the off-axis cracks, where strong tensional fields are present. The propagation of delaminations leads to a further decrease in stiffness, which is however usually lower than that due to the saturation of the off-axis cracks.

iii Fibre breakage. From a macroscopic point of view, the final event of damage is represented by the breakage, understood as separation in two or more parts, of the laminate. This phenomenon is usually controlled by the breakage of the fibres of the more layers that are oriented the most with the external load. Figure 6 shows damage evolution, the steps mentioned before are clearly visible.

Figure 6: Damage evolution on a glass-epoxy laminate. [15]

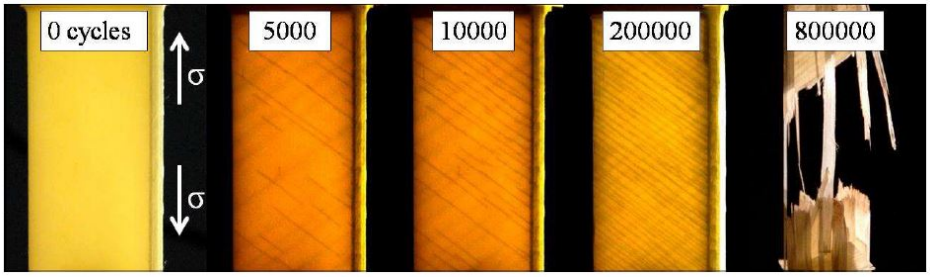


## 2.3 Fatigue Testing Method

Fatigue limit and stress-life S-N curve are widely used to characterize fatigue properties. Speaking about composites, fatigue limit is the value of applied stress that leads to failure at a high number of cycles, $10^6 \sim 10^7$. The most common approach to determine the fatigue limit of a material is the staircase approach. It consists of a series of tests at various stress amplitudes. Given an initial stress amplitude and a "step height" of the so-called staircase, specimens are then tested in sequence. If at a certain loading amplitude the specimen reaches $10^6$ cycles,the stress level is raised to the next step and the successor is tested. If the specimen fails, its successor is tested one step lower. And so on.

The *S-N* curve is a plot of magnitude of applied stress $S$ against cycles at failure $N$.

This process of material characterization is time consuming and its costs are relevant. Not to mention that results can be different at various loading frequencies, stress ratios, surface roughness values, manufacturing processes, size of structure. CFRP composites are more complicated than metals the number of variables that account in fatigue damaging process is hard to manage. Therefore, rapid evaluation of fatigue behavior of CFRP composites is of great importance, especially for lightweight structural design. [6]

## 2.4 Determination of Fatigue Limit Based on IRT Data

Determination of fatigue limit based on IRT data is an idea that firstly had been applied to metals. Recent studies have come out with faster techniques to come to a result. This topic is of great interest for design engineers since reducing costs and time of material characterization can boost their activities.

### 2.4.1 Theoretical Framework

Fatigue is an irreversible process of degradation occurring in a material subjected to cyclic loading that may culminate in cracks or complete fracture after a sufficient number of fluctuations. Degradation mechanisms of composite materials produce a large amount of heat. Irreversible changes of CFRP composites under cyclic loading are matrix cracking, crack propagation, debonding, delamination and fibre breakage. Damage evolution process is connected to energy dissipation. The accumulation of dissipated energy causes temperature variations that can be observed and measured on the surfaces of the materials by an infrared camera. Using of infrared thermography (IRT) to locate fatigue damage in materials is a common non-destructive evaluation (NDE) technique. The thermographic approach for determining the fatigue limit is an idea developed initially by Risitano and co-workers [11]. Thermography, in this context, consists in pointing an infrared camera at the specimen during a fatigue test.The physical phenomenon behind this application is the radiation emission of an object. The output is a time-dependent contour map of the surface of the specimen. The recorded images are then analyzed to determine temperature evolution, to locate damage initiation and to detect damage propagation. In figure 7 a photo of experimental setup of infrared instruments for fatigue tests. Numerous experiments and research agree to identify a common behavior of composites when subjected to cyclic loading. Surface temperature of a specimen or a component undergoing an alternating stress above its fatigue limit and below its yield limit can be divided in three phases, as it is presented

Figure 7: Setup of thermography measurements on fatigue test [11]

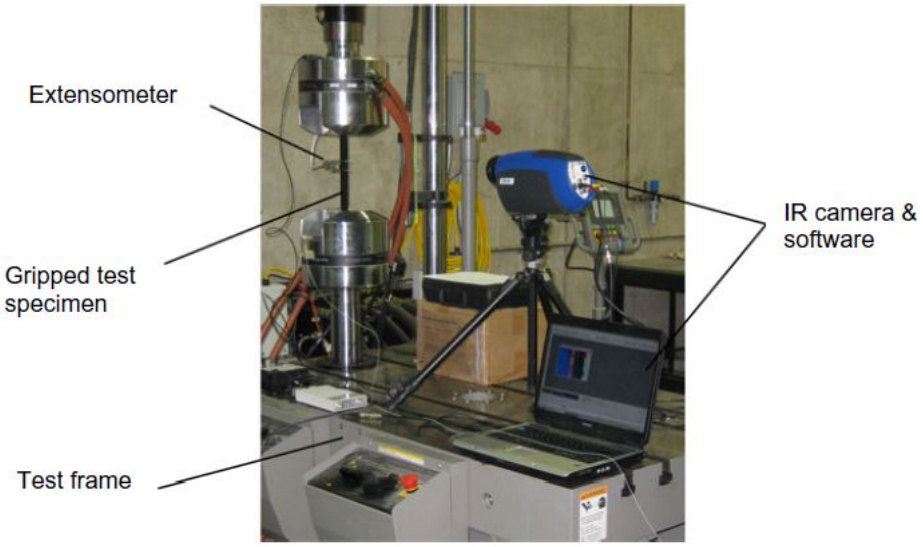


in figure 8:

Figure 8: Distinction of the three phases on a T against N plot [8]

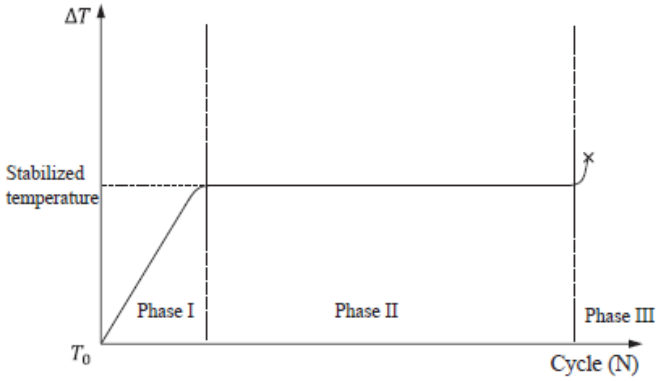


I Initial temperature increase

II Temperature stabilization

III Abrupt temperature increase before final failure

Phase I consists in a rapid increase of temperature, it accounts for less than 10% of fatigue life. Temperature of the specimen raises from ambient temperature ($T_0$) to a

higher stabilized temperature

Phase II is a plateau, temperature stabilizes at a certain value. The material achieves a dynamic thermal equilibrium between heat generation and dissipation. This part accounts for more than 90% of specimen's life.

Phase III corresponds to a rapid temperature increase. It is an extremely unbalanced stage, damage propagates quickly and structural integrity of the specimen is compromised. This part come to an end in $10^3$ cycles.

Another peculiar aspect is that this three-phases pattern changes shape according to the stress level. For example, at higher loads, stabilized temperature is higher and life is shorter, as showed in Figure 9. Correlation between $\Delta T_{stab}$ and stress amplitude

Figure 9: Different temperature evolution at different stress levels [9]

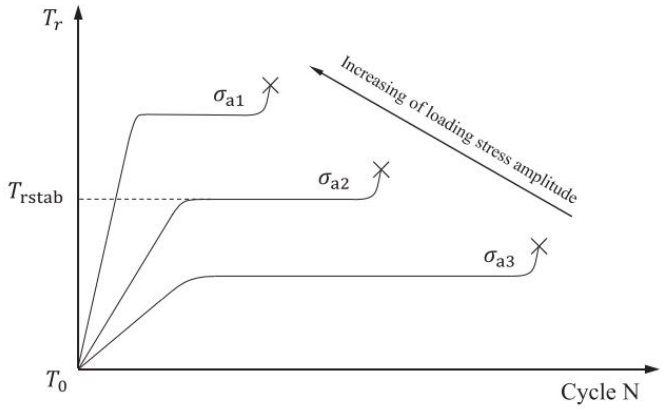


$\sigma_a$ is a crucial property in order to determine fatigue limit. To acquire values of stable increased temperature, this stepped loading pattern can be adopted. After a certain number of cycles, when temperature stabilizes, value of $\Delta T_{stab}$ is obtained and it is possible to move to another loading amplitude, as shown in Figure 10a. This process is shorter than a fatigue test of a single specimen and the output is a plot of $\Delta T_{stab}$ vs $\sigma_a$ (Figure 10b), which is the first step of the application of rapid methods for determining fatigue limit. [6]

Figure 10: a) Step loading pattern b) $\Delta T_{stab}$ vs $\sigma_a$ plot

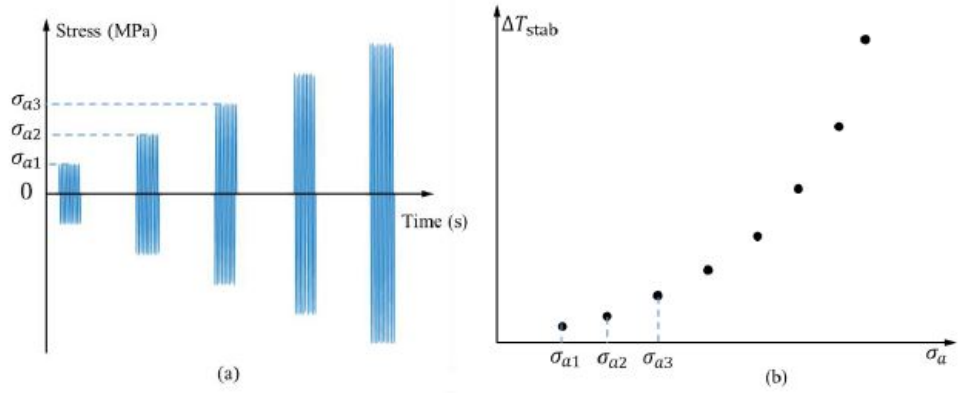


### 2.4.2 Traditional Methodologies

Once the plot of $\Delta T_{stab}$ vs $\sigma_a$ is acquired, how can the fatigue limit be determined with precision and uniqueness? Authors have different definitions for the fatigue limit concerning this temperature-stress correlation, figure 11 shows .

Figure 11: Comparison of TCM and OCM methods [9]

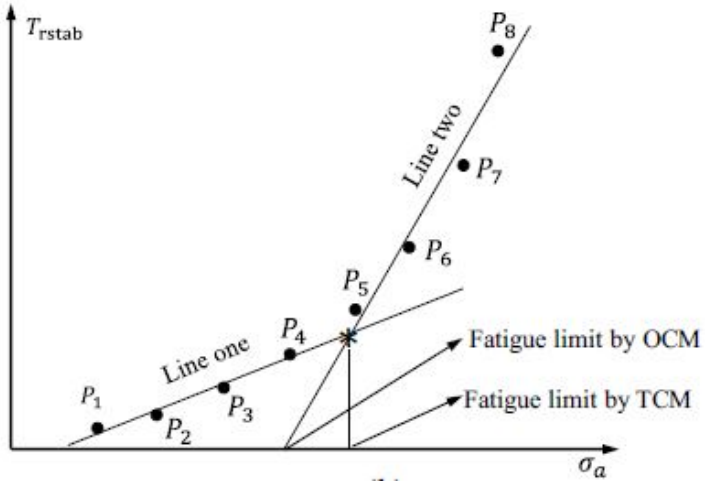


Luong et al. propose to interpolate graphic data with two lines, one related to stresses below and one to stresses above the fatigue limit (Two-Curve Method, TCM). The x-coordinate of the intersection gives the stress amplitude corresponding to the fatigue limit. Risitano's method assumes fatigue limit as the intersection of the second line (above fatigue limit) and x-axis (One-Curve Method, OCM).[9]

# 3 Existing models

In this context many models have been developed, some just concern the graphical choice of the fatigue limit, some others go further, they are able to describe the whole S-N curve. Models often agree on the definition of thermodynamics aspects that are the involved in the problem, but given the purpose of this work, and based on the most recent literature I chose two models to analyse. This way even thermodynamic description of the phenomena involved is in discussion.

## 3.1 Huang's Model

Huang [8] has recently set up a complete model to face the determination S-N curve in a very rapid way. This allows to get to a solution in 3 days, with an important save on costs. Its model is complete in every aspect, from the determination of the fatigue limit to the proposition of a new stiffness degradation model, from the description thermodynamic aspects involved in this context to the numerical model of material.

### 3.1.1 Theoretical overview

This model starts from two concepts:

- Damage mechanism in CFRP subjected to fatigue loading are: matrix cracking, fibre/matrix interface cracking, fibre breakage and delamination.
- Damage leads to stiffness degradation

It is pointed out that stiffness degradation is a preferable parameter to characterize development in a component under cyclic loading. That is because damage accumulation process has a relevant correlation with the evolution of temperature measured by IRT. Damage evolution can be divided into three stages:

1 In stage 1 damage grows quickly, micro-cracks appear in the matrix or in the matrix/fibre interface. Also some fibres break during the first cycles, those are fibres which present some defects and for that they have poor strength.

2 Stage 2 begins at a point of saturation of the early damages. Degradation continues slowly and regularly. Delamination and matrix cracking are the phenomena involved here.

3 Stage 3 shows a rapid degradation process: fibres break and the stiffness of the laminate is compromised. It lasts usually less than 1000 cycles.

An analogy between damage accumulation profile and temperature profile can be set. Stage 2 of this process accounts for the largest part of number of cycles and has a stable trend. It can be deduced a relationship between $\Delta T_{stab}$ and the damage accumulation rate. Damage index employed in this model is defined as follows:

$$D^*(N) = \frac{K_0 - K(N)}{K_0 - K_f^*} = \frac{1 - k(N)}{1 - k_f^*} \tag{1}$$

where $D^*$ is cumulative damage and $N$ is the current number of cycles. $K_0$, $K(N)$ and $K_f^*$ are the stiffness - Young's Modulus - of the specimen of virgin material, at $N^{th}$ cycle and at the final cycle right before failure (failure threshold stiffness) $N_f^*$, respectively. $k(N)$ defined as $K(N)/K_0$ is the normalized stiffness at $N^{th}$ cycle and $k_f^*$, defined as $K_f^*/K_0$ is the normalized failure threshold stiffness. Its value goes from 1 - virgin material - and then it decreases. Figure 12 illustrates these concepts. For practical reasons, the stiffness degradation mode undergoes two simplifications:

- Stage 3 is neglected. This because it is a short period and it involves an unstable damage propagation where stiffness is not easy to measure. So only stage 1 and 2 are considered and $N_f$ is defined as number of cycles at the end of stage 2. Likewise, $k_f$ is referred to normalized stiffness degradation at $N_f$

- Given two specimens with same stacking sequence, geometry and manufacturing process, subjected to cyclic loading at fixed loading frequency and stress ratio, the

Figure 12: Three stages of damage accumulation [7]

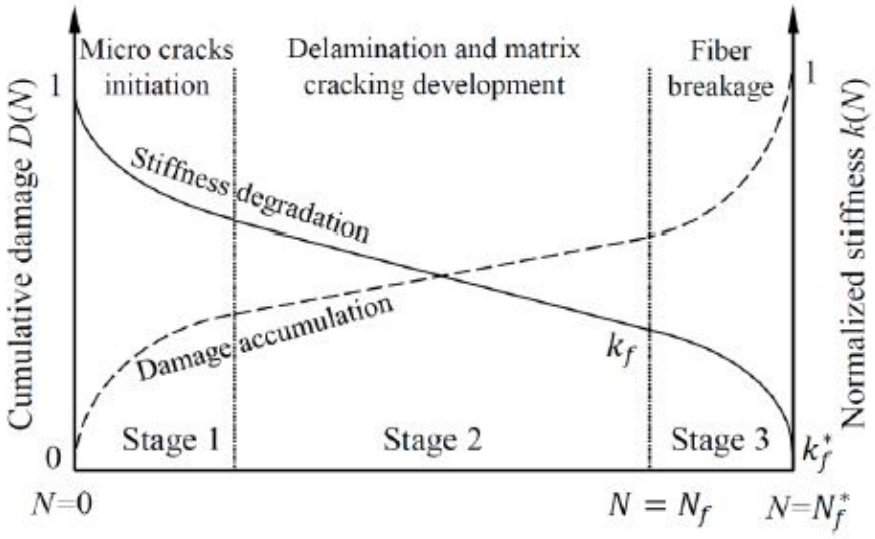


normalized values of failure threshold stiffness $K_f^*$ are considered independent of the maximum loading stress level. This has been proven in previous research [18]. So, also the $k_f$ corresponding to the end of stage 2 is considered independent of the maximum loading stress level. After simplifications on Eq. (1) a new relation can be set:

$$D(N) = \frac{1 - k(N)}{1 - k_f} \tag{2}$$

In order to use the correlation between self-heating and damage evolution it comes necessary to quantify the normalized stiffness degradation as a function of cycle number. Huang proposes this law to associate the two quantities:

$$k(N) = 1 - p\Delta T_{stab} N^{1/q} (q \geq 1) \tag{3}$$

where parameters $p$ and $q$ are material properties, independent of temperature and loading cycles. Since $k(N)$ is a normalized value, it is dimensionless. Consequently dimension of $p$ is [°C×Cycle$^{1/q}$] and q is dimensionless. These two parameters are calibrated using a surface interpolation of experimental data, the output of this process is shown in Figure 13. The term $q$ controls the shape of the normalized stiffness degradation function. $\Delta T_{stab}$, as mentioned before, is function of the applied stress. The term

Figure 13: Surface fitting on MATLAB to calibrate $p$ and $q$ parameters [7].

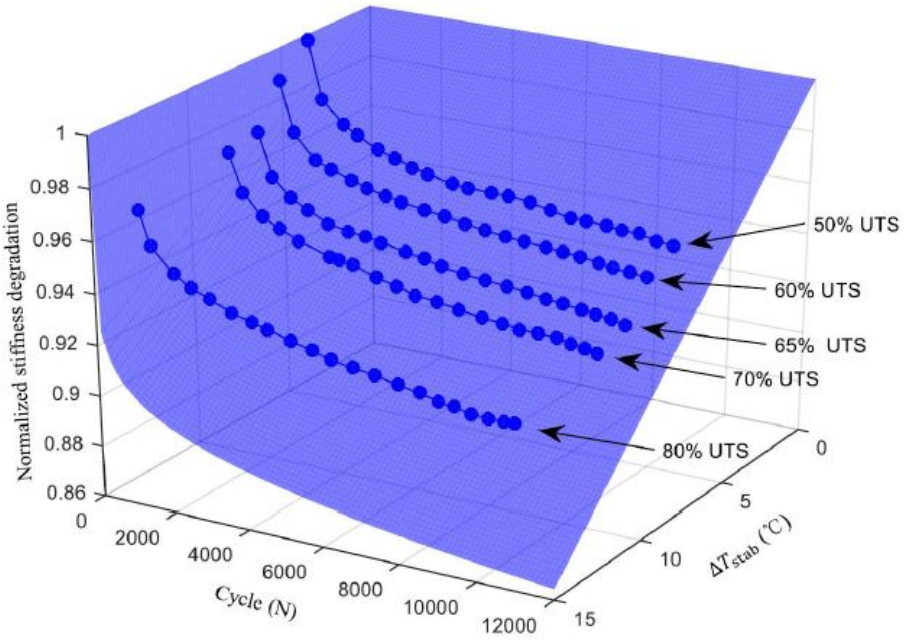


$q$ filters the influence of $\Delta T_{stab}$. The function has an initial rapid decrease and then a stable decrease, it describes the same shape of the experimental data.

The combination of Eq.(2) and (3) gives a new expression of the damage index:

$$D(N) = \frac{p\Delta T_{stab} N^{1/q}}{1 - k_f} (q \geq 1) \tag{4}$$

It is remarkable that through other operations, that are not the focus of this work, in [7] the final expression that leads to the prediction of the whole $S - N$ curve can be obtained:

$$N_f = (\frac{1 - k_f}{pf(\sigma)} \tag{5}$$

This study goes further, also the thermodynamics of the phenomenon are taken into account: damage evolution process is correlated to energy dissipation. The accumulated dissipated energy is one of the causes of temperature variation [1]. According to the concepts of classical thermodynamics of irreversible process, combining first and second principle of thermodynamics, the local heat equation is expressed as:

$$\rho C\dot{T} + Q_{tf} = d_1 + s_{the} + sic + r_e \tag{6}$$

where:

i $\rho C\dot{T}$ is the heat storage rate characterized by temperature change. $\rho$ is mass density and $C$ is specific heat capacity, they are material constants, independent of internal states. T is temperature.

ii $Q_{tf}$ = -div($k$ grad $T$) is the heat loss rate from the material to the ambient. It includes all the conduction, convection and radiation effects. $k$ is heat transfer coefficient.

iii $d_1$ is called the intrinsic dissipation mechanical source. [3].

iv $s_{the}$ is the thermoelastic source. Temperature variation is due to adiabatic variation of volume of elastic materials:

v $s_{ic}$ is the internal coupling source. It denotes the heat source induced by the coupling effect between internal variables and temperature.

vi $r_e$ is the external heat supply.

Per unit of volume, the quantities $d_1$, $s_{the}$ and $s_{ic}$ are:

$$d_1 = \sigma : \mathbf{D} - \rho\psi_{,\varepsilon} : \dot{\varepsilon} - \rho\psi_{,\alpha} \cdot \dot{\alpha} \tag{7}$$

$$s_{the} = \rho T\psi_{,T,\varepsilon} : \dot{\varepsilon} \tag{8}$$

$$s_{ic} = \rho T\psi_{,T,\alpha} \cdot \dot{\alpha} \tag{9}$$

$d_1$ is the difference between the anelastic energy rate $w_a$' = $\sigma$:**D** - $\rho$ $\psi_{,\varepsilon}$:$\dot{\varepsilon}$ and the stored energy rate $w_s$' = $\rho\psi_{,\alpha} \cdot \dot{\alpha}$. $\sigma$ is the Cauchy stress tensor, **D** is the Eulerian strain rate tensor,$\psi$ the specific Helmoholtz free energy, $\varepsilon$ the strain tensor, $\alpha$ are state variables. As stated before, $Q_{tf}$ includes the three heat transfer mechanisms.
The local transferred energy is:

$$Q_{tf} = -\lambda S_{section}\nabla^2 T + \beta\frac{S_{surface}}{V}(T - T_{room}) + \kappa\sigma\frac{S_{surface}}{V}(T^4 - T_{room}^4) \tag{10}$$

Where V is the control volume, $S_{section}$ is the area of the section of the specimen in the control volume V, $S_{surface}$ is the area of exposed surface in the control volume V. Figure 14 shows a schematic representation of these quantities. $\lambda$, $\beta$ and $\kappa$ are respectively thermal conductivity, convection coefficient and surface emissivity. $\zeta_n$ is Stefan-Boltzmann constant.

Figure 14: Control volume of a flat specimen [8]

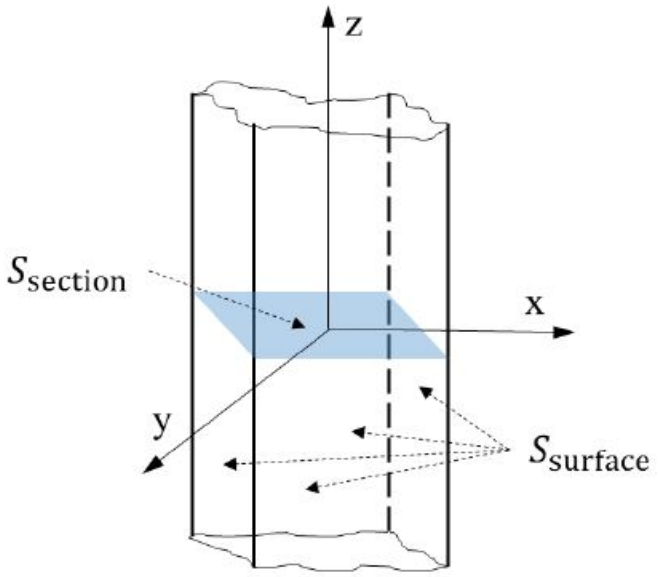


In order to simplify Eq. 6 these hypothesis are set:

- Specimens are subjected to homogeneous uniaxial tests.
- Mass density $\rho$, specific heat capacity $C$ and heat transfer coefficient are material constants, independent of the internal states.
- The coupling heat source between internal variables and temperature - $s_{ic}$ - is neglected because only small temperatures variations are considered and such variations have no influence on microstructural state. Fatigue is considered a purely dissipative mechanism.
- $r_e$ is time-independent and its influence can be removed by installing reference specimens in the room.

- The heat source distribution is uniform at any time within the specimen gauge part.

Now considering a single cycle and integrating both sides of Eq.(6), this expression can be obtained:

$$\int_t^{t+1/f} \rho C\dot{T} + \int_t^{t+1/f} Q_{tf} = \int_t^{t+1/f} d_1 + \int_t^{t+1/f} s_{the} + \int_t^{t+1/f} s_{ic} + \int_t^{t+1/f} r_e \quad (11)$$

Under the hypothesis mentioned before and noting the relation can be simplified to:

$$\int_t^{t+1/f} Q_{tf} \approx \int_t^{t+1/f} d_1 \quad (12)$$

Another approximation is to consider that the specimen spends the whole fatigue life in a Phase II condition (it is true for about 90% of life). This way total dissipated heat $H_d$ during the whole fatigue life can be estimated by:

$$H_d = N_f \int_t^{t+1/f} d_1 \quad (13)$$

Where $N_f$ is again the number of cycles at the end of Phase II.

### 3.1.2 Numerical model

Since it is not easy to measure the heat loss rate directly by IRT camera during fatigue tests, Huang set up a numerical simulation to quantify the total dissipated heat. The main hypothesis is considering that the heat generation is induced by two quantities: internal friction and damage mechanisms (delamination and crack propagation). It is also assumed, by applying the definition used in engineering, that the fatigue limit is the threshold of applied loading stress: below it, no damage occurs, infinite life is granted and all the heat generation is due to internal friction; above it, material degradation happens at some rate, life is limited and heat generation can be seen as the sum of internal friction and damage propagation.

In this point of view, fatigue limit is the point that splits in two the curve of Figure 15. Blue part indicates the portion of heat generation rate related to only internal friction. Red part is the portion related to delamination and crack propagation.

One important observation is about how the border line is obtained and why the trend has that shape. It is assumed that internal friction can be described through a quadratic polynomial function of loading amplitude. Only the points before the fatigue limit are used to fit the curve, then the prosecution sets the border between the two zones. Once the two zones are divided, the heat generation related to damage can be

Figure 15: Heat generation rate induced by internal friction and delamination and crack propagation are divided [8]

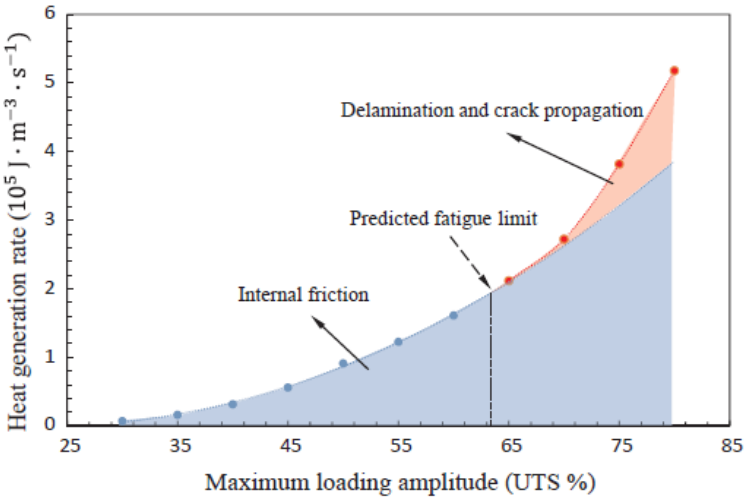


quantified as a difference between the value of the total heat generation rate and the one related to internal friction. Starting from total dissipated heat per unit of volume related to damage $H_{d\_damage}$, fatigue limit can be predicted in a way that matches well with experimental data. It is supposed that $H_{d\_damage}$ is independent of loading stress, i.e. constant. Figure 16 shows how the order of magnitude of $H_{d_damage}$ is the same at different loading amplitudes. Since heat generation rate induced by damage $Q_{d\_damage}$ can be considered as a function of loading amplitude:

$$Q_{g\_damage} = g(\sigma_a) \tag{14}$$

Figure 16: Heat generation related to damage per unit of volume calculated through numerical model [8]

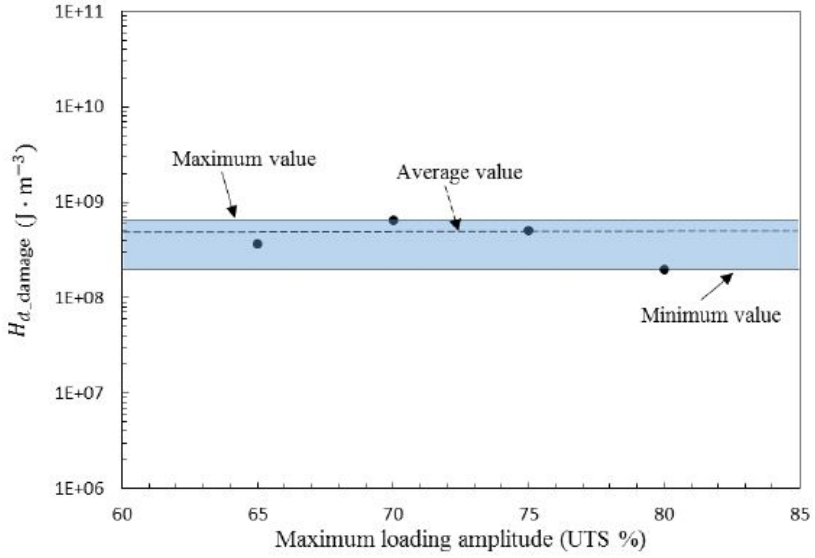


Number of cycles is expressed as:

$$N_f = \frac{f H_{d\_damage}}{g(\sigma_a)} \tag{15}$$

And so *S-N* curve, which is the main goal of this process, can be obtained. Comparing the calculated area with the experimental data it can be deduced that most of the predicted area of the model lies in the scope of 95% confidence interval, as presented in Figure 17.

## 3.2 Mahmoudi's Method

Recent studies of Mahmoudi and Mohammadi [13] propose a different point of view on the situation. The purpose is as well to predict life of composite materials in a rapid way and considering the thermo-mechanical behaviour of the component while subjected to cyclic loading.

Figure 17: Comparison of experimental data and predicted $S - N$ curve [8]

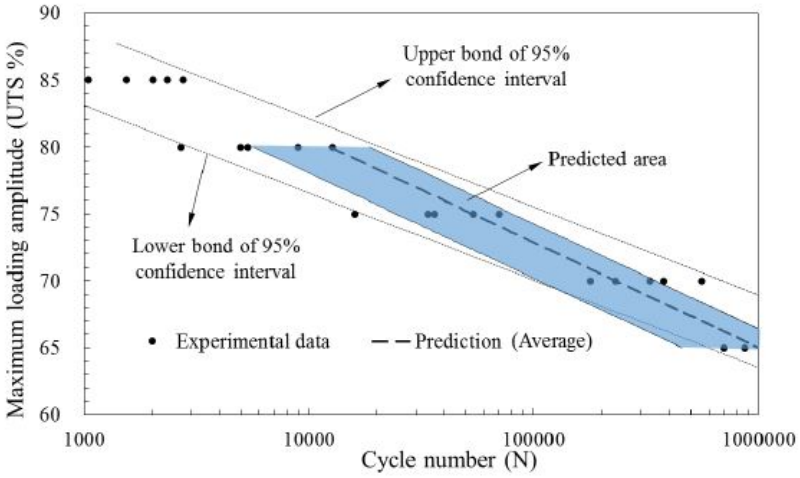


### 3.2.1 Theoretical overview

The model considers fatigue as an irreversible thermodynamic process, the starting point is the first principle of thermodynamics:

$$\frac{dE}{dt} = \frac{dW}{dt} + \frac{dQ}{dt} \tag{16}$$

where t is time, E is total energy referred to a control volume and Q and W are work and heat flow across the surfaces of the control volume. Considering small deformations for a specimen under cyclic loading the equation can be written in terms of specific quantities:

$$\rho\frac{de}{dt} = \sigma : \dot{\varepsilon} - div\vec{q} \tag{17}$$

where $\rho$ is mass density, e is specific internal energy, $\sigma$ is stress tensor, $\dot{\varepsilon}$ is strain rate and $\vec{q}$ is the heat flux.

Helmoltz free energy (HFE) is considered related to two internal variables and one observable variable, elastic strain and damage parameter are internal, temperature is the observable one.

$$\psi = \psi(\varepsilon^e, T, \omega) = e - Ts \tag{18}$$

where $\varepsilon^e$ is elastic strain and $T$ is temperature, s is entropy per volume and $\omega$ is damage parameter, that is going to be defined later. Differentiating Eq. 18 with respect to t,

this new relation can be written:

$$\frac{\partial \psi}{\partial t} = (\frac{\partial \psi}{\partial \varepsilon^e}) : \dot{\varepsilon}^e + (\frac{\partial \psi}{\partial T})\dot{T} + (\frac{\partial \psi}{\partial \omega})\dot{\omega} \tag{19}$$

That can be simplified into [13]:

$$\sigma : \dot{\varepsilon} - \sigma : \dot{\varepsilon}^e + Y\dot{\omega} = \rho C\dot{T} - k\nabla^2 T \tag{20}$$

where $C$ is the specific heat capacity, k is the heat conductivity and $Y = -\frac{\partial \psi}{\partial \omega}$.

Assuming small deformations, $\sigma : \varepsilon\dot{0}0 - \sigma : \dot{\varepsilon}^e$ is replaced by $\sigma : \dot{\varepsilon}^i e$ where $\dot{\varepsilon}^i e$ is the rate of inelastic deformations. The internal generated heat due to inelastic deformations is divided in irreversible work due to irreversible strains, $W_p = \sigma : \dot{\varepsilon}^p$, and internal friction caused by the viscoelastic nature of the polymeric matrix, $W_f$. This assumption leads to this formulation:

$$\dot{W}_p + \dot{W}_f + \dot{E}_d = \rho C\dot{T} + \dot{E}_{diss} \tag{21}$$

Where $\dot{E}_d$ is the damage energy rate and $\dot{E}_{diss} = -k\nabla^2 T$ is the heat dissipation through specimen. Equation 21 can be written in a way to point out the temperature variation:

$$\dot{T} = \frac{\dot{W}_p + \dot{W}_f + \dot{E}_d - \dot{E}_{diss}}{\rho C} \tag{22}$$

In conclusion, this thermo-mechanical model separates the sources of heat in irreversible work, damage energy and internal friction. In order to achieve the topic of the present work, this model is taken into account because it adds complexity to the description of the phenomena.

Irreversible work $W_p$ is modelled following a method presented by Ladeveze and LeDantec [17]. The main hypothesis is that there is no damage and irreversible deformation in the fibre direction.

$$\widetilde{\sigma} = v \begin{pmatrix} \sigma_{11} \\ \frac{\langle \sigma_{22} \rangle}{1-\omega_2} - \langle \sigma_{22} \rangle_- \\ \frac{\sqrt{2}\sigma_{12}}{1-\omega_{12}} \end{pmatrix} \tag{23}$$

with:

$$\begin{aligned} \langle a \rangle_+ &= a if a \geq 0; otherwise \langle a \rangle_+ = 0 \\ \langle a \rangle_- &= a if a \leq 0; otherwise \langle a \rangle_- = 0 \end{aligned} \tag{24}$$

where $\sigma_{11}$, $\sigma_{22}$ and $\sigma_{12}$ are the components of stress through fibre, orthogonal to fibre and shear direction. $\omega_2$ is damage parameter related to matrix, $\omega_{12}$ is damage parameter in shear direction.

A new function is defined:

$$f = \sqrt{\widetilde{\sigma}_{12}^2 + a^2 \widetilde{\sigma}_{22}^2} - R(p) - R_0 \tag{25}$$

It defines the elastic domain of the material. R is a function of the accumulated plastic strain $p$, $R = R(p)$ and it is a material-characteristic function. $a^2$ is a material constant. The condition of $f < 0$ corresponds to the elastic domain, while $f = 0$ and $\dot{f} = 0$ correspond to plastic domain. $R_0$ is the initial threshold value. Strain hardening curve of the material can be obtained from:

$$R(p) + R_0 = \sqrt{\frac{\sigma_{12}^2}{1 - \omega_{12}} + \frac{a^2 \sigma_{22}^2}{1 - \omega_2}} \tag{26}$$

$R(p)$ is simplified as :

$$R(p) = \beta p^{\alpha} \tag{27}$$

where $\alpha$ and $\beta$ are material parameters. The yield conditions are:

$$\begin{aligned} \dot{\widetilde{\varepsilon}}_{11}^p &= 0 \\ \dot{\widetilde{\varepsilon}}_{22}^p &= a^2 \frac{\widetilde{\sigma}_{22}}{R(p) + R_0} \dot{p} \\ \dot{\widetilde{\varepsilon}}_{12}^p &= \frac{\widetilde{\sigma}_{12}}{2(R(p) + R_0)} \dot{p} \end{aligned} \tag{28}$$

$$\dot{p} = \frac{\sigma_{12} \dot{\sigma_{12}} + a^2 \sigma_{22} \dot{\sigma_{22}}}{(R(p) + R_0) \frac{\partial R}{\partial p}} \tag{29}$$

This way, irreversible work dissipation - $W_p$ - is formulated as follows:

$$W_p = \widetilde{\sigma}_{ij} \dot{\widetilde{\varepsilon}}_{ij}^p = \sigma_{ij} \dot{\varepsilon}_{ij}^p = \sigma_{22} \dot{\varepsilon}_{22}^p + 2\sigma_{12} \dot{\varepsilon}_{12}^p \tag{30}$$

In this model, internal friction is defined as the phenomenon of heat generation caused by the viscoelastic nature of polymeric matrix of the composite. According to the common theory of viscoelasticity and dynamic damping behavior of polymeric materials, if the input is a sinusoidal strain with frequency $w$ like $\varepsilon(t) = \varepsilon_0 cos(wt)$, it can be expressed in complex notation as:

$$\varepsilon(t) = \varepsilon_0 e^{i(wt)} \tag{31}$$

The response is a stress oscillating with the same frequency but leading the strain by a phase angle $\delta$ as:

$$\sigma(t) = \sigma_0 cos(wt + \delta) \; or \; \sigma(t) = \sigma_0 e^{i(wt+\delta)} \tag{32}$$

Thanks to the complex notation, a complex modulus can be defined:

$$E^* = \frac{\sigma_0}{\varepsilon_0}(\cos\delta + i\sin\delta) = E_1 + iE_2 = |E^*|e^{i\delta} \tag{33}$$

where $E_1$ and $E_2$ are storage and loss modulus. The energy produced in one cycle $W_f$ can be obtained by integrating work over a cycle period $T_c$

$$W_f = \int_0^{T_c} \sigma \frac{d\varepsilon}{dt} dt = \int_0^{T_c} \sigma_0 \varepsilon_0 w \sin wt \cos(wt + \delta) dt = \pi \sigma_0 \varepsilon_0 \sin\delta \tag{34}$$

The third component of heat generation is called damage energy. This quantity needs a damage energy model to calculate damage parameters and the related damage forces during fatigue loading. The authors present a continuum-damage model (CDM) that updates damage properties at each cycle [16]. According to this study, damage parameters are defined as:

$$\omega_k = \frac{E_{k0} - E_k}{E_{k0}} \tag{35}$$

where k stands for m or f, referring to matrix or fibre. $E_{k0}$ is the stiffness of the virgin material, $E_k$ is the stiffness of the material at the actual time.

Damage evolution per cycle is described by this damage evolution law:

$$\frac{d\omega_k}{dN} = \frac{A_k \Delta Y_k^{B_k}}{(1-\omega_k)^{C_k}} \tag{36}$$

Where A,B and C are material constants. N is the number of cycles and $\Delta Y_k$ is the variation of the thermodynamic force during each loading cycle: $\max Y_k - \min Y_k$. The thermodynamic forces, that are defined as $Y = -\frac{\partial \psi}{\partial \omega}$, can be quantified as:

$$\begin{aligned} Y_f &= \frac{1}{2}\frac{[\sigma_{11}^f \varepsilon_{11}^f + \sigma_{22}^f \varepsilon_{22}^f]}{1-\omega_f} \\ Y_m &= \frac{1}{2}\frac{[\sigma_{11}^m \varepsilon_{11}^f + \sigma_{22}^m \varepsilon_{22}^m]}{1-\omega_m} \end{aligned} \tag{37}$$

Now the damage energy rate can be calculated as:

$$\dot{E}_d = Y_f \dot{\omega}_f + Y_m \dot{\omega}_m \tag{38}$$

The term of heat dissipation is the sum of three components: conduction, convection and radiation:

$$\dot{E}_{diss} = \dot{E}_{cond} + \dot{E}_{conv} + \dot{E}_{rad} \tag{39}$$

And by assuming a constant ambient temperature and uniform temperature for gauge section, Eq 39 can be expressed as:

$$\dot{E}_{diss} = \frac{2kA_{cond}}{V}\frac{\Delta T}{\Delta z} + [h(T_s - T_a) + e\beta(T_s^4 - T_a^4)]\frac{A_{surf}}{V} \tag{40}$$

Where $A_{cond}$ is the cross-sectional area, $A_{surf}$ is the gauge section surface, $\Delta T/\Delta z$ is the temperature gradient between gauge section and grips of the testing machine, $k$ is thermal conductivity, $h$ is convective heat transfer coefficient, $e$ is surface emissivity and $\beta$ is Stefan-Boltzmann constant.

# 4 Representative Volume Elements

In order to investigate what stress and strain distributions are involved at the micromechanical level, it is required a new simulation instrument. Huang and Mahmoudi developed numerical models of homogeneous CFRP composites, as presented in figure 18, where plies are made of unidirectional layers that share the same properties all along the geometry: Since these are not models that can quantify values at microscopic level,

Figure 18: Numerical model of Huang: an example of homogeneous model

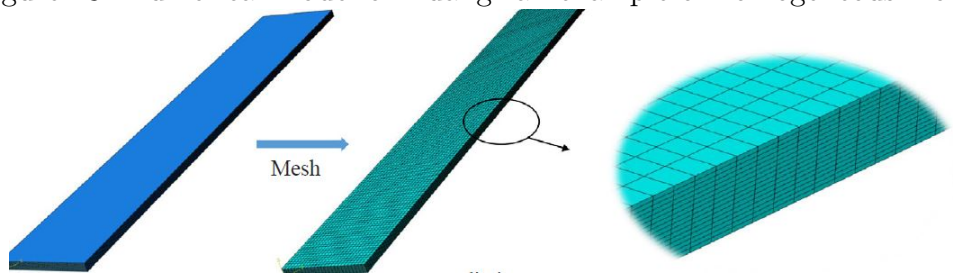


in the present work a Representative Volume Element (RVE) based model is set up.

## 4.1 Overview

An RVE is the smallest material volume for which the macroscopic constitutive representation is a sufficiently accurate model to represent mean constitutive response [4]. The RVE has to be modelled in a way that duplicating it it provides sufficient accuracy of representing the material's larger scales, as it is shown in figure 19: Facing the homogenisation issue, the first conditions to be set are uniform strains at the microscale RVE. This way, mechanical behavior of the composite can be calculated. Then, Periodic Boundary Conditions (PBCs) are necessary to generate the deformation of the surrounding elements. They are called "periodic" because they ensure that even when deformed, the external surfaces remain periodic. Figure 20 shows this concept. In this work, the modelling of these elements has been carried on by using commercial finite element software ABAQUS. This choice has some benefits: control on RVE geometry

Figure 19: Representation of a matrix-fibre composite component made of multiplied RVEs [10]

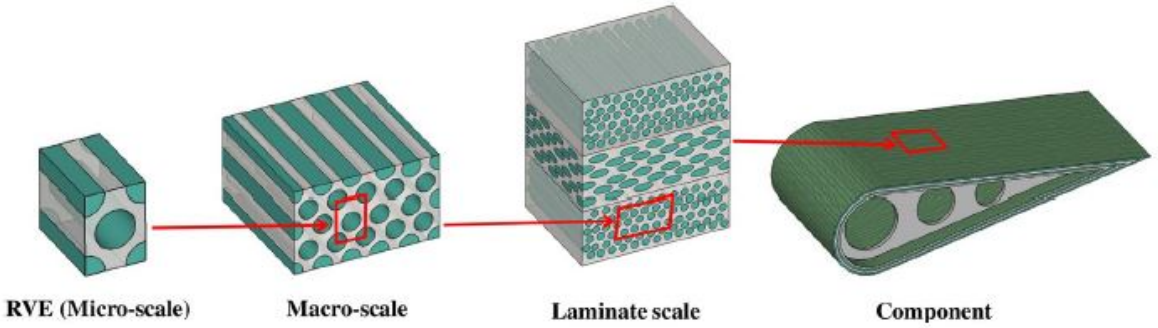


Figure 20: RVEs after loading have periodic deformations

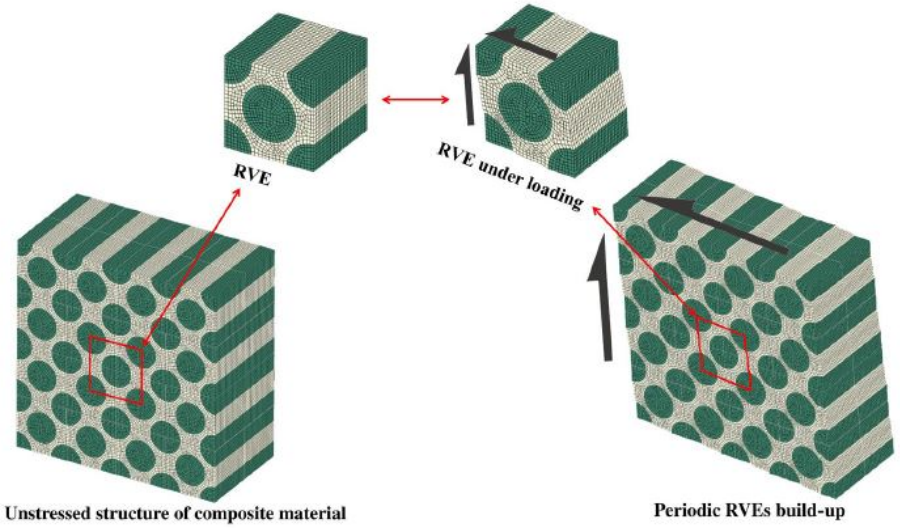


is very accurate and managing large quantities of results is simple.

## 4.2 Periodic RVE homogenisation

The idea of RVE homogenisation is to impose uniform strains to the volume elements in order to obtain the effective mechanical behavior. For heterogeneous materials like composites, mechanical properties of the RVE depend firstly on volume fraction of fibres and secondly on the disposition of fibre and matrix inside the RVE [2].

In the present work three conditions are taken into account. Given the coordinate system presented in Figure 21, they can be defined as:

Figure 21: Coordinate system of the RVE [10]

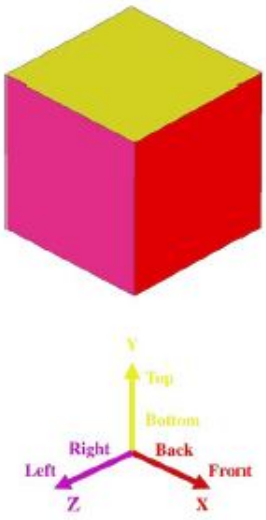


i Deformation on the x axis: the front face is pulled and a strain is imposed. Periodic Boundary Conditions of this case are:

$$\begin{aligned} X_{Front} - X_{Back} &= 1 \\ X_{Top,Left} - X_{Bottom,Right} &= 0 \\ Y_{Top,Front,Left} - Y_{Back,Bottom,Right} &= 0 \\ Z_{Front,Top,Left} - Y_{Back,Bottom,Right} &= 0 \end{aligned} \tag{41}$$

ii Deformation on the y axis: the top face is pulled and a strain is imposed. Periodic Boundary Conditions of this case are:

Figure 22: Direction 11 deformation [10]

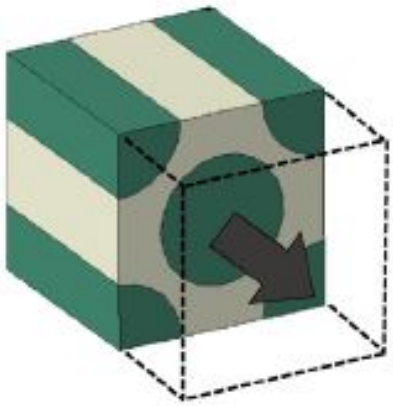

Figure 23: Direction 22 deformation [10]

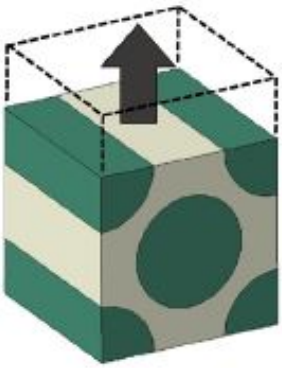

$$
\begin{aligned}
Y_{Top} - X_{Bottom} &= 1 \\
Y_{Top,Left} - Y_{Bottom,Right} &= 0 \\
Z_{Top,Front,Left} - Z_{Back,Bottom,Right} &= 0 \\
X_{Front,Top,Left} - Z_{Back,Bottom,Right} &= 0
\end{aligned}
\tag{42}
$$

iii Shear deformation on the x-y axes: top and front faces are pulled by an imposed shear strain. Periodic Boundary Conditions of this case are:

Figure 24: Direction 12 deformation [10]

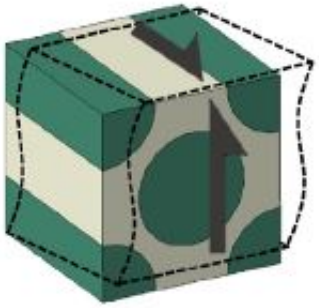

$$
\begin{aligned}
X_{Front,Left} - X_{Back,Right} &= 0 \\
Y_{Front} - Y_{Back} &= 1 \\
X_{Top} - X_{Bottom} &= 1 \\
Y_{Top,Left} - Y_{Bottom,Right} &= 0 \\
Z_{Front,Top,Left} - Z_{Back,Bottom,Right} &= 0
\end{aligned}
\tag{43}
$$

Practically, the mentioned conditions are not applied to geometrical entities but they are applied to the nodes of the meshed part. This step is schematised in Figure 25:

Figure 25: Map of the meshed volume [10]

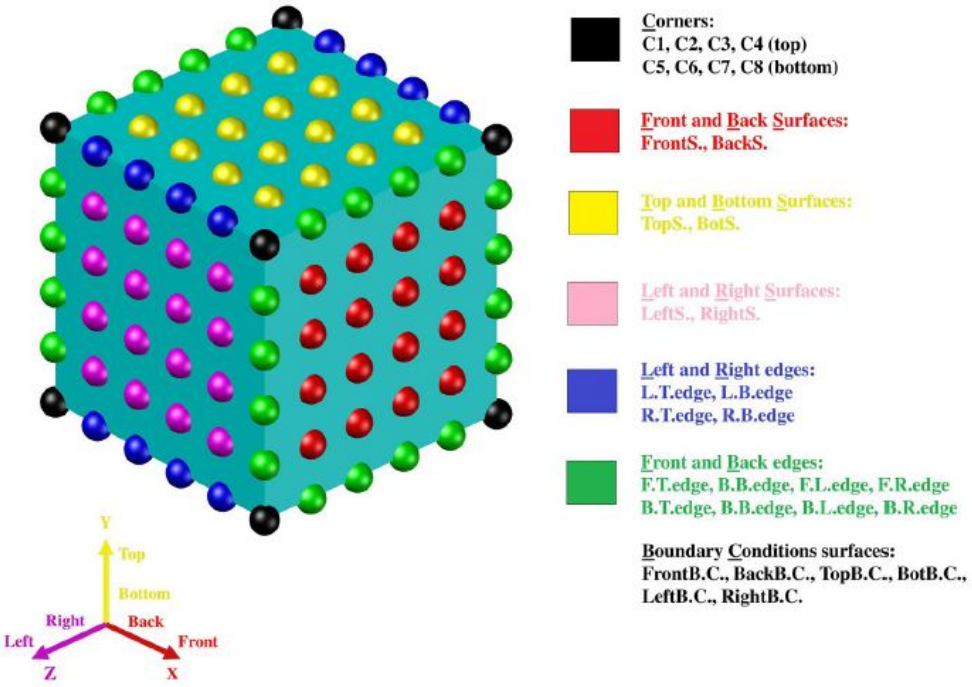

# 5 New Developed Model

The complexity of phenomena that occur when a CFRP specimen is subjected to cyclic loading requests an accurate analysis. In literature it is still not clear how to correlate damage evolution and energy dissipation. The approaches that are commonly used for metals can not be applied to composites. Research is moving in different directions. The present work, considering the models and the techniques explained above, has the goal of quantifying the energies related to different phenomena during the fatigue test. The idea is to get to an order of magnitude of the energies, so, in future tests, those quantities can be correlated to objective observations. This issue requires a micromechanical model, since damage of composites can only be explained by analysis at this level. What is limiting empirical research on this issue, at the present day, is technology. There is no way to measure very small temperature variations, for example.

## 5.1 Theoretical overview

This model bases its theoretical setting on Mahmoudi's model[13]. Eq 22 is the thermodynamic description of the temperature variation. The element of novelty is that quantities are not calculated analytically but through a micromechanical simulation (RVE). The idea is to run numerous simulations, one every 500 or 1000 cycles at the beginning and less frequent later, and every time adjust the settings to the up-to-cycle values. Given the accuracy of the model, material properties and their evolution are the primary focus in order to obtain reasonable data.

Here a brief comparison of positive and lacking aspects of the models:

| Huang's Model | Mahmoudi's Model |
|---|---|
| Predicts S-N curve | Predicts S-N curve |
| Material is modelled as homogeneous | Material is modelled as homogeneous |
| Macroscopic scale | Macroscopic scale |
| Energy sources are split only in two categories | Energy sources are separated in multiple categories |
| Elastic modulus is function of stress amplitude and number of cycles | Elastic modulus is function exclusively of the number of cycles |

The model presented in this work first of all brings the analysis to the microscopic scale. This way, fibre and matrix are modeled separately and ,for example, phenomena like stress peaks can be evaluated. In addition, energy sources are separate in different categories and they are related to fibre and matrix independently. Another positive aspect is that mechanical properties are both function of stress amplitude and number of cycles. This is the flowing chart of the simulations:

i Set fibre orientation.

ii Set the composite layup.

iii set $\sigma_{max}$ as a percentage of the UTS of the laminate.

iv Fatigue tests are stress controlled; normally the stress ratio is R=0.1. $\sigma_{min}$ and $\sigma_{avg}$ are obtained.

v First cycle: N=1; $\omega_f$,$\omega_m = 0$.

vi From data of Young's Modulus $E = E(N = 1)$, laminate stiffness is set

vii Plastic behavior, if present, is added to the elastic strain.

viii Total strain, elastic plus plastic, is imposed to the RVE

ix Outputs are $\sigma_{11f}$, $\sigma_{22f}$, $\sigma_{12f}$, $\sigma_{11m}$, $\sigma_{22m}$, $\sigma_{12m}$, $\varepsilon_{11f}$, $\varepsilon_{22f}$, $\varepsilon_{12f}$, $\varepsilon_{11m}$, $\varepsilon_{22m}$, $\varepsilon_{12m}$.

x Irreversible work $W_p$ and damage energy $E_d$ related to fibre and matrix separately are calculated.

xi Process is repeated by point v) for $N = 500, 1000, 5000...$

xii Process is repeated by point i) for different fibre orientations, layup and $\sigma_{max}$.

## 5.2 RVE simulations

Numerical simulations of the RVE are based on these hypothesis:

- Isotropic materials: it is true that the simulation is non homogeneous, but fibre and matrix, taken separately, are homogeneous and isotropic.
- Matrix has elastoplastic behavior while fibre only operates in the elastic domain.
- No debonding or cracking: implementing those features requires other analysis.
- Periodic Boundary Conditions: Eqq. 41, 42 and 43 are converted into boundary conditions of the RVE

The main settings of the simulations are:

- Element dimensions: 1mm x 1mm x 1mm
- Mesh type: Hex
- Mesh dimension: 0.065mm
- Element type: C3D8R (brick element)
- $E_{fibre} = 220$ GPa
- $E_{matrix} = 2.6$ GPa
- Displacement, not stress, is imposed

### 5.2.1 Material characterization

Material characterization is the most important part of the simulation. Output values depend on these inputs. Not only the properties of the virgin material are requested, but also their evolution during fatigue test.

### 5.2.2 Matrix - Epoxy EPL1012

The epoxy resin used in the CFRP composites data collected by Huang and Mahmoudi is an EPL1012. Elastoplastic behavior of the matrix is described with a bi-linear function. The first part is controlled by the elastic modulus and then, after PEL (proportionality limit point), the second is controlled by the plastic modulus. Figure 26 shows the bi-linear plot. UTS is at 71 MPa and PEL is at 46 MPa. Elastic modulus

Figure 26: Stress-strain plot of the elastoplastic behavior of the resin

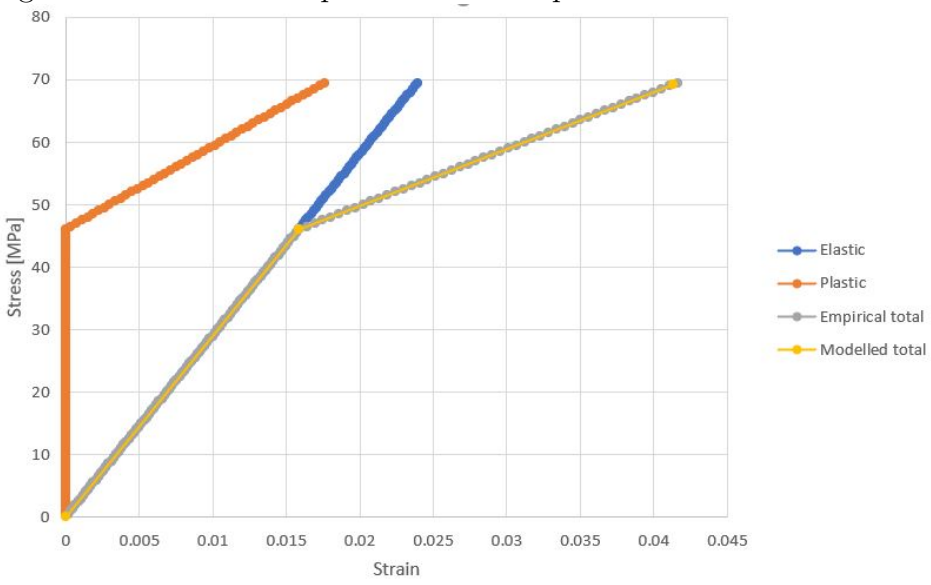


is 2.6 GPa while plastic modulus is 911 MPa. Poisson's ratio is 0.353. Data of matrix

properties come from [12] where several tests on epoxy resin specimens were conducted. Properties are referred to behavior under traction.

According to Mahmoudi's work, matrix has the stiffness degradation pattern presented in Figure 27. The other parameters: $A_m$, $B_m$ and $C_m$ are obtained as follows.

Figure 27: Damage index and normalized Young modulus of matrix

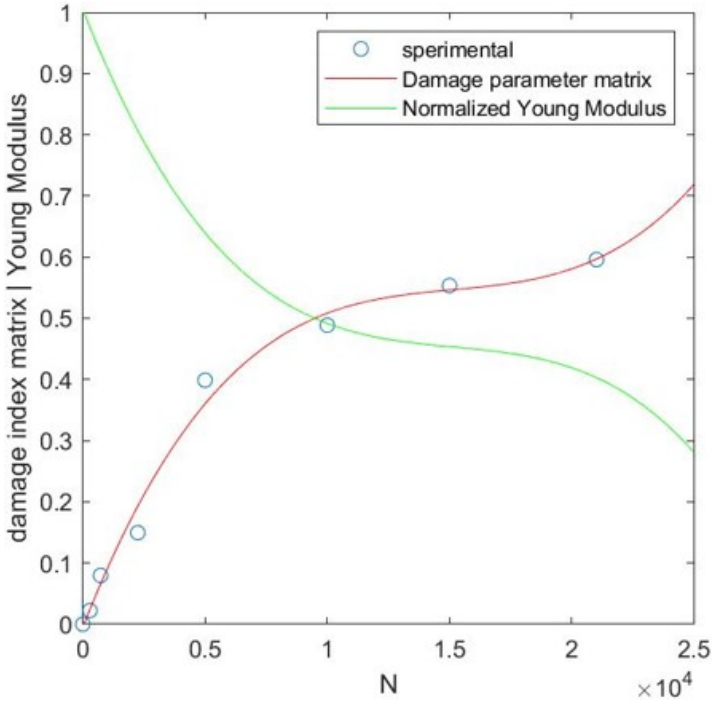


Starting from Eq. 36, this relation can be written:

$$\frac{d\omega_k}{dN} = \frac{A_k}{(2E_k)^{B_k}} \frac{\sigma_{max,k}^{2B_k}}{(1-\omega_k)^{2B_k+C_k}} \tag{44}$$

where $\sigma_{max,k}$ is the magnitude of applied maximum stress in stress controlled test. By integration of this equation from $\omega = 0$ to $\omega = \omega_{c,k}$ this expression is obtained:

$$\sigma_{max,k}^{2B_k} N_f = \frac{(2E_k)^{B_k}}{A_k(2B_k + C_k + 1)} (1 - (1 - \omega_{c,k})^{2B_k+C_k+1}) \tag{45}$$

where $\omega c, k$ is critical value of damage. Taking logarithm of the both sides a new relation between logarithmic life and logarithmic maximum applied stress is obtained:

$$\log N_{f,k} = x + y \log \sigma_{max,k} \tag{46}$$

Therefore, $B_k$ is determined through Eq. 46 and the experimental data, from the slope of $\log N_k$ versus $\log \sigma - max, k$ diagram. Then, $A_k$ and $C_k$ are determined starting from taking logarithm of both the sides of Eq. 44:

$$\log \frac{d\omega_k}{dN} = \log(\frac{A_k}{(2E_k)^{B_k}}\sigma - max, k^{2B_k} + (2B_k + C_k)\log(1-\omega_k)^{-1} \tag{47}$$

and then following these steps:

- plot $\omega_k$ versus $N$
- determine the slope of $\omega_k$ versus $N$
- calculate $\log \frac{d\omega_k}{dN}$ and $\log(1-\omega_k)$
- plot $log\frac{d\omega_k}{dN}$ versus $\log(1-\omega_k)^{-1}$

From the slope and the intercept of the last plot $A_k$ and $C_k$ are obtained[16].

Plastic domain of the material is obtained through pure shear tests:

Figure 28: Plot of $R(p) + R_0$ vs $p$

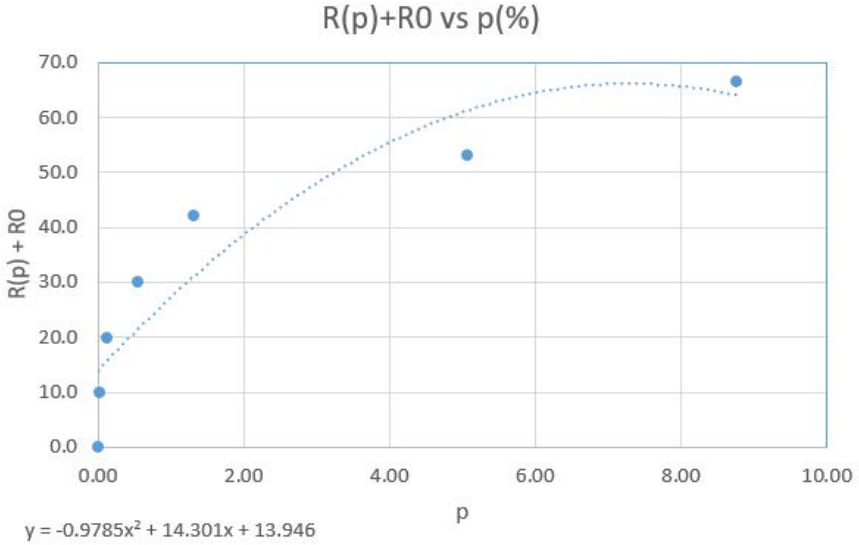


$R_0$, $\alpha$ and $\beta$ are obtained plotting the quantities presented in figure 28 and figure 29 and fitting data with the relations presented in section 3.2.1.

Figure 29: Plot of $\log(R(p))$ vs $\log p$

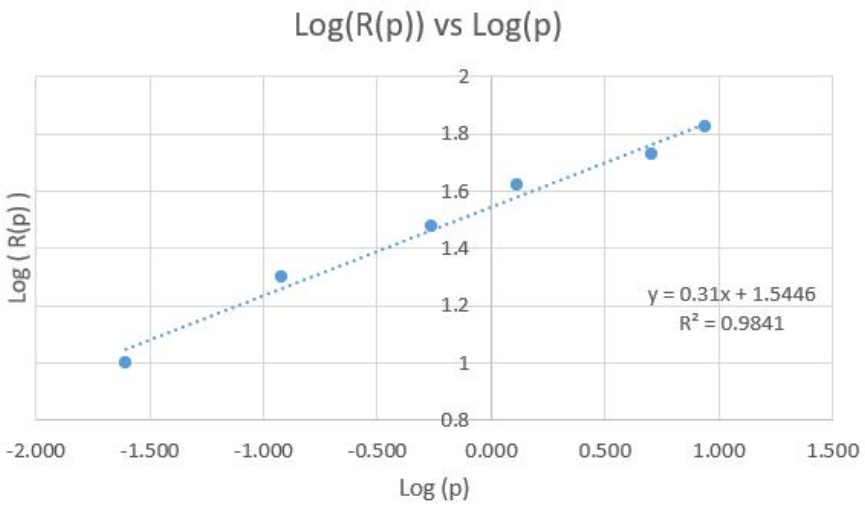


### 5.2.3 Fibre - Carbon T300

The carbon fibre used in the CFRP composites data collected by Huang and Mahmoudi is a T300. Its behavior is considered completely elastic. "Toray Composite Materials America" shares its data on T300, as shown in Figure 30. Only Poisson's ratio is not mentioned here, a value of 0.27 is adopted, according to general statistics on carbon fibres

### 5.2.4 Simulation details

The RVE is sketched as a cylinder included inside a cube(Figure 31). The dimensions of the cube are 1mm x 1mm x 1mm while the cylinder has a radius of 0.418mm. This value is calculated in order to guarantee the respect of the Volume fraction $V_f = 0.55$. Fibre and matrix are considered two features of the same part.

Two different materials are created:

- Fibre, that shows elastic behavior. It is isotropic.
- Matrix, in which are implemented both the elastic and plastic behaviors. In

Figure 30: Table of mechanical properties of T300 carbon fibre

**FIBER PROPERTIES**

| PROPERTY | ENGLISH | METRIC | METHOD |
|---|---|---|---|
| Tensile Strength | 512 ksi | 3,530 MPa | TY-030B-01 |
| Tensile Modulus | 33.4 Msi | 230 GPa | TY-030B-01 |
| Strain at Failure | | 1.5% | TY-030B-01 |
| Density | | 1.76 g/cm$^3$ | TY-030B-02 |
| Filament Diameter | | 7 µm | |
| Yield | 1K | 66 g/1000m | TY-030B-03 |
| | 3K | 198 g /1000m | TY-030B-03 |
| | 6K | 396 g /1000m | TY-030B-03 |

Figure 31: Sketch of the two phases

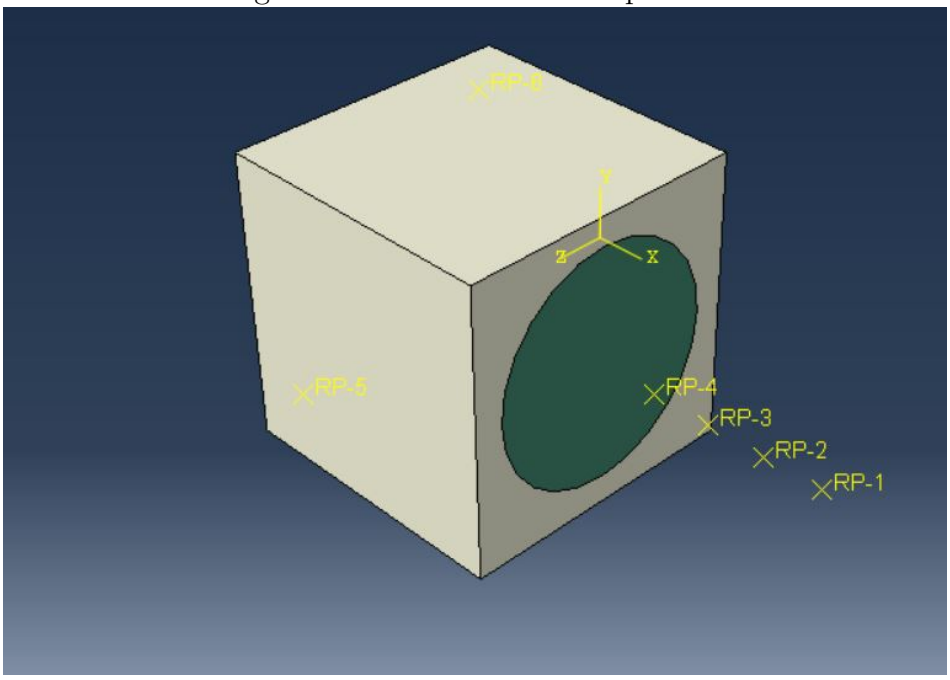


ABAQUS plastic behavior is defined as a curve starting from the threshold value. It is isotropic.

The cyclic loading is simulated as a cyclic strain at the RVE scale.The simulation

runs one cycle every time. The frequency of the load is 6 Hz. The max amplitude of the stress is a percentage of the UTS and this value is a variable. Given the stress ratio of 0.1, all the necessary parameters to describe the stress are available. Since the load applied is a sinusoidal function, the strain is a sinusoidal function as well. The strain oscillation of every cycle is calculated by imagining of imposing the corresponding stress to the hole laminate:

$$\varepsilon_{RVE}(t) = \varepsilon_{lam}(t) = \frac{\sigma(t)}{E_{lam}|_N} \tag{48}$$

The cycle amplitude, which is a consequence of the stiffness evolution of the material, increases from the first cycles to the latest.

In order to apply this condition to the RVE it is necessary to create a new step. Its time period is 169 in relation to the time in seconds of a cycle, given the frequency of 6 Hz.

Meshing the component, as presented in Figure 32 is not a difficult task in this case, only few observations are needed:

- The mesh is entirely made of hexahedrons. The geometry is suitable for this choice.
- The element type is a brick, C3D8R. The solid element is the ideal to simulate behavior of massive materials.
- Mesh dimension is 0.065mm. This value came at the end of an iterative process. It is the right balance between accuracy and computational cost.
- A final check on the meshed part is always necessary. The ideal situation is that every element has the same shape of the theoretical element, a cube in this case. Taking a look at Figure 33 the mesh is pretty accurate, the distortions are generated by the necessity of dealing with the circumference.

Figure 32: Meshed part

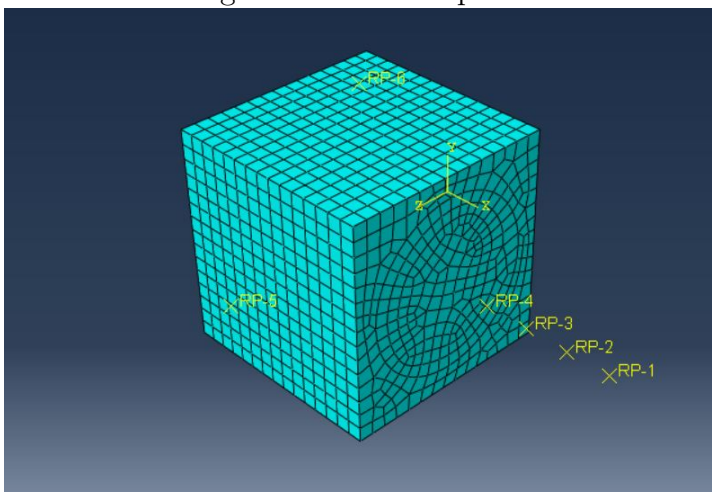


Figure 33: Detail of hex mesh

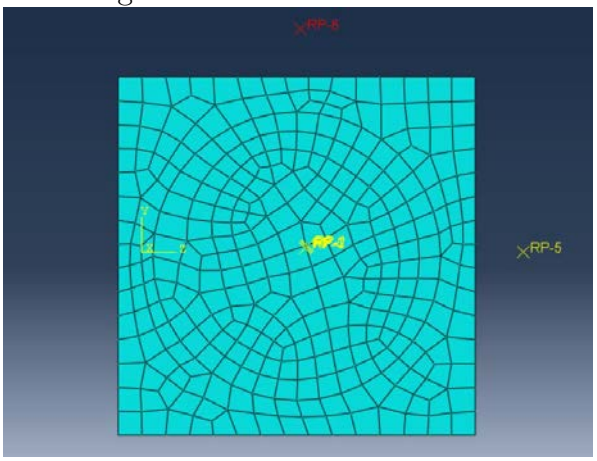

# 6 Results

The results of this work are multiple: results of the RVE simulation, validation of the RVE model and heat generation energy quantification.

## 6.1 Simulation results

The output are stresses and strains in 11,12,22 direction related to matrix and fibre. The nodal values referred to the matrix are averaged among all the nodes of the matrix set, which includes all the elements of the cylinder. The nodal values referred to the fibre are averaged among all the nodes of the fibre set, which includes all the element of the cube, except for the cylinder.Three types of simulations are carried on:

1 Simulation 1 concerns an RVE subjected to strain in direction 11.

Stresses in 11 direction are high and concentrated on the fibre. This is in according with the theory that indicates the fibre as the mainly loaded phase when the composite faces a load oriented with the fibre direction. Matrix is almost unloaded.

Stresses in 22 direction are low but not negligible. A symmetric distribution pattern can be noted. Lateral sides of the matrix are in traction while vertical sides are in compression. It is related to the effect of Poisson's coefficient.

Stresses in 12 direction are really low. Saying that stresses are null is correct.Little variations of the tension are visible on the contoured map but effectively they do not mean anything relevant.

2 Simulation 2 concerns an RVE subjected to strain in direction 22.

Stresses in direction 22 are symmetrically distributed, for effect of the geometry of the RVE. On the vertical sides of the matrix, traction is dominant while on the lateral sides compression is more present. There is not a significant difference of tensions between matrix and fibre.

Figure 34: Strain in direction 11, stress in direction 11

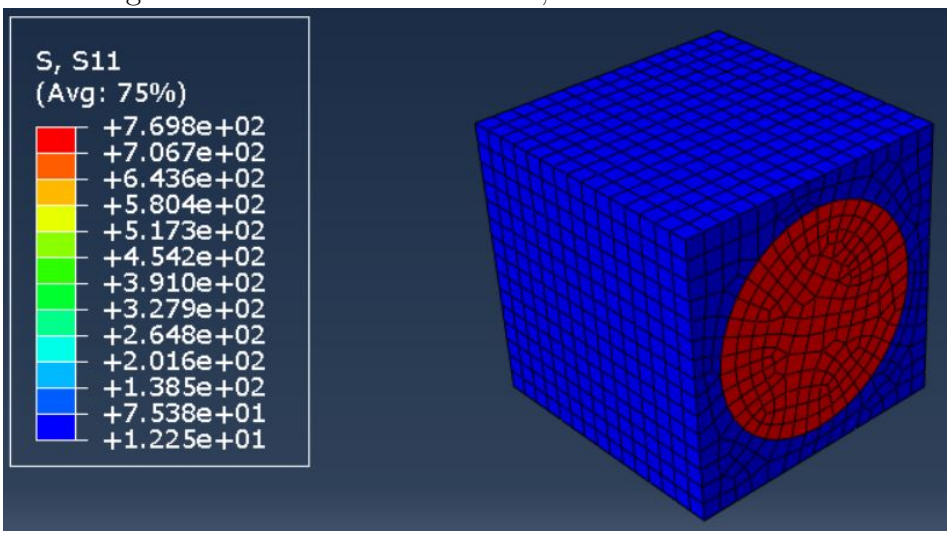


Figure 35: Strain in direction 11, stress in direction 22

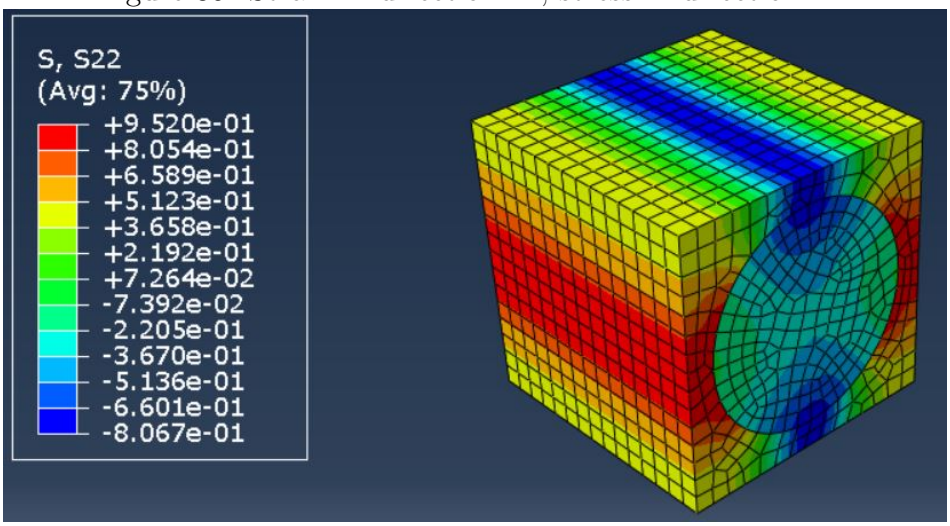


Stresses in direction 11 are symmetrically distributed as well. Fibre is in compression while matrix is only stressed in the middle area of the faces.

Stresses in direction 12 are null. Values in traction and compression are not significant. Little variations of colors are not an issue, given the order of magnitude.

3 Simulation 3 concerns an RVE subjected to strain in direction 12.

Stresses in direction 11 are null. There is no difference on the stress of fibre and

Figure 36: Strain in direction 11, stress in direction 12

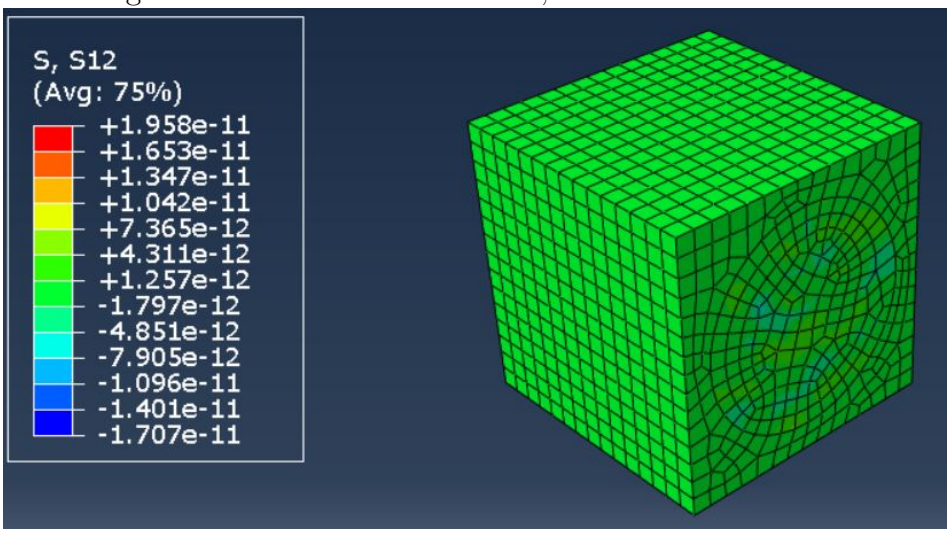


Figure 37: Strain in direction 22, stress in direction 22

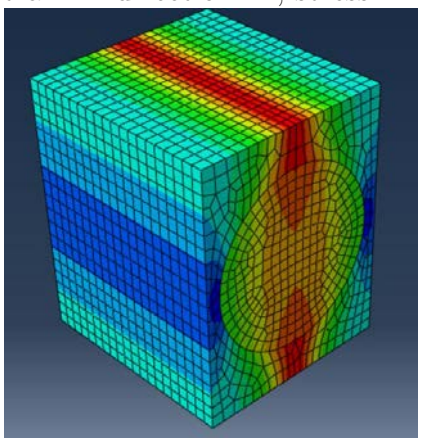

matrix, values are not significant.

Stresses in direction 22 are null. Values are not significant and the small differences of color are not relevant.

Stresses in direction 12 are disposed in a symmetrical pattern. There is tension in the strained faces, while the other faces are subjected to tension of the opposite sign.

These results are in complete accord with the theory and the physical sense of the phenomena. The shapes are exaggerated in order to make the deformed geometry more

Figure 38: Strain in direction 22, stress in direction 11

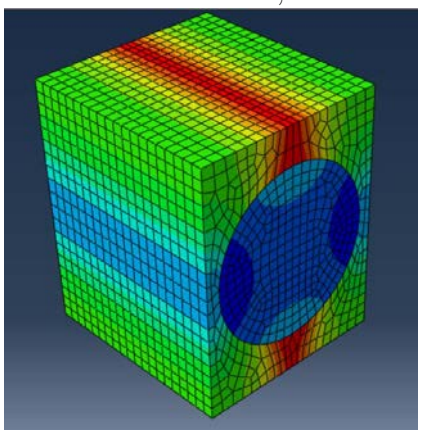

Figure 39: Strain in direction 22, stress in direction 12

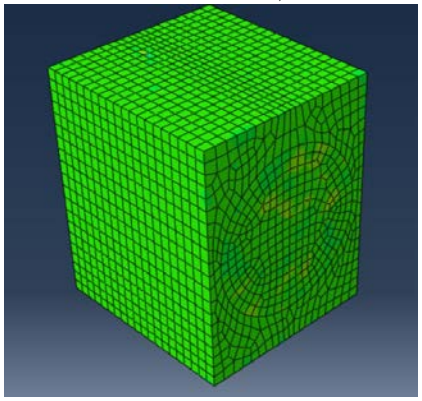

Figure 40: Strain in direction 12, stress in direction 11

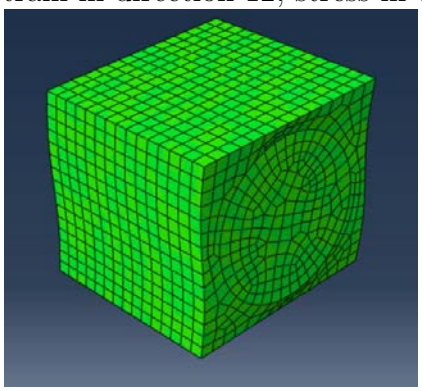

visible. By the way, the contour plot is accurate and data do not exceed in any case UTS limits or maximum strains of the materials. It can be deduced that the RVE simulation is correct and that this part of the model is validated.

Figure 41: Strain in direction 12, stress in direction 22

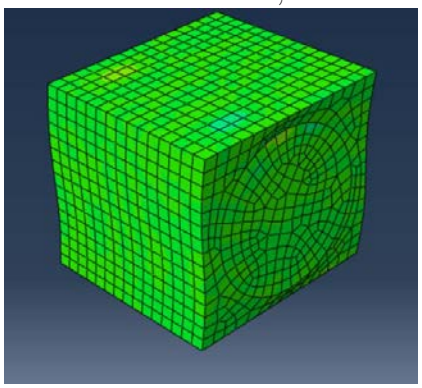

Figure 42: Strain in direction 12, stress in direction 12

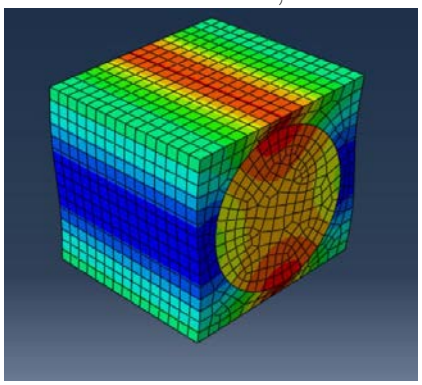

## 6.2 Heat generation results

The goal of this part was to recreate the heat generation data of Mahmoudi in order to validate the model and then apply it to Huang's material data. Mahmoudi heat generation data can not be recreated reliably. Another aspect is that the stress level considered in these data is always above the fatigue limit, so a complete discussion of the model is not possible.

### 6.2.1 Internal friction

Figure 43 shows the energy rate due to internal friction vs number of cycles based on Mahmoudi energy data. Figure 44 shows the same quantity, calculated with the new proposed model. The difference is huge. Two orders of magnitude are extremely

Figure 43: Energy rate due to internal friction, Mahmoudi

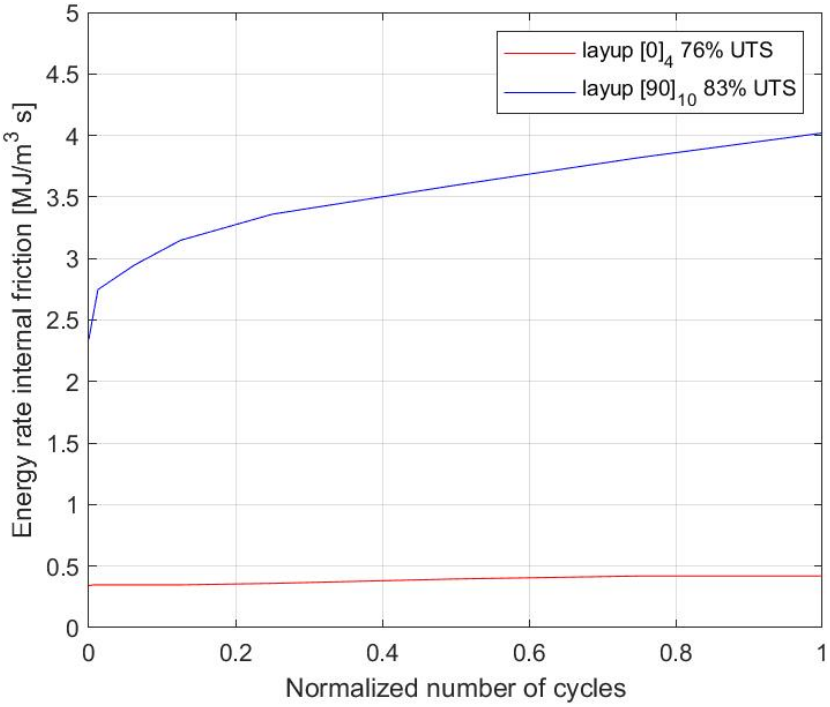


Figure 44: Energy rate due to internal friction, present work

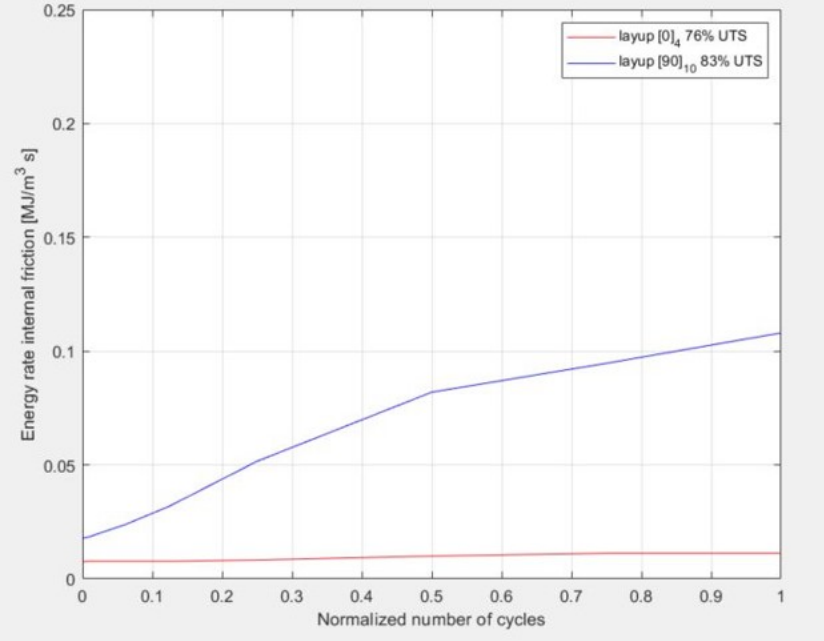

relevant. What can be happened is that the stress computed in the equation was the stress of the whole laminate. That is wrong because the cause of internal friction, which is defined as heat generation due to the viscoelastic nature of the polymeric matrix must be computed with quantities referred only to the matrix. A part from the values the trend is similar but the shape is not exactly the same.

### 6.2.2 Damage work

This part does not present a mismatch of values between the two models. Figure 45 shows the plot of energy rate due to damage work vs number of cycles. An interesting aspect is that the value is almost constant. There is a sort of balancing effect because damage parameter decreases but derivative $d\omega/dN$ balances the oscillations. What is remarkable is that according to this model the largest part of the damage energy is correlated to matrix. And here, there is a quantity, an energy related to damage of the matrix. This is a great point of the present work.

Figure 45: Energy rate due to damage work, present work

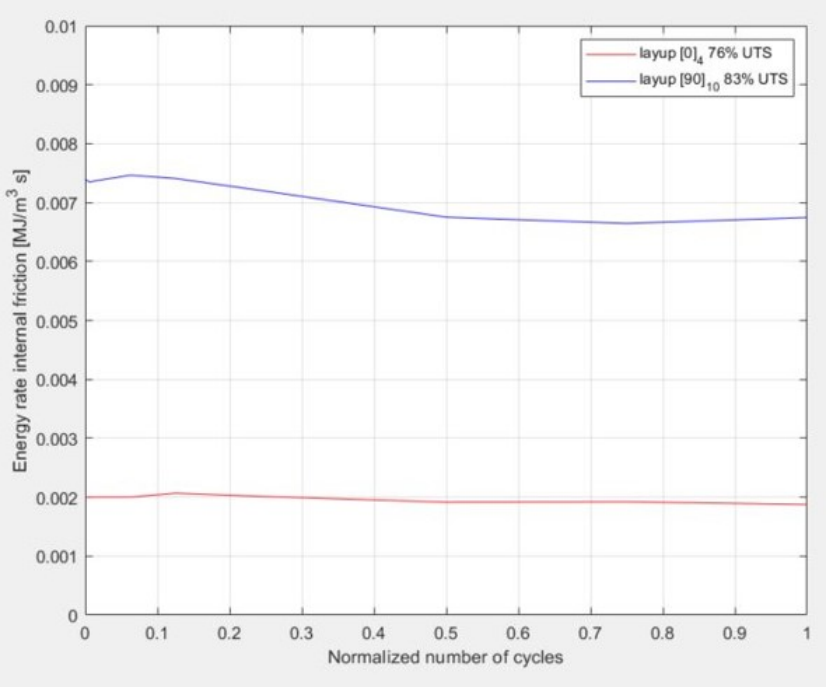

### 6.2.3 Irreversible work

This part does not show a difference between Mahmoudi's and this work's plot of energy rate due to irreversible work. Figure 46 shows the plot. These results are only referred to [90°] laminates because one hypothesis is that there is no irreversible work in fibre direction.

Figure 46: Energy rate due to irreversible work, present work

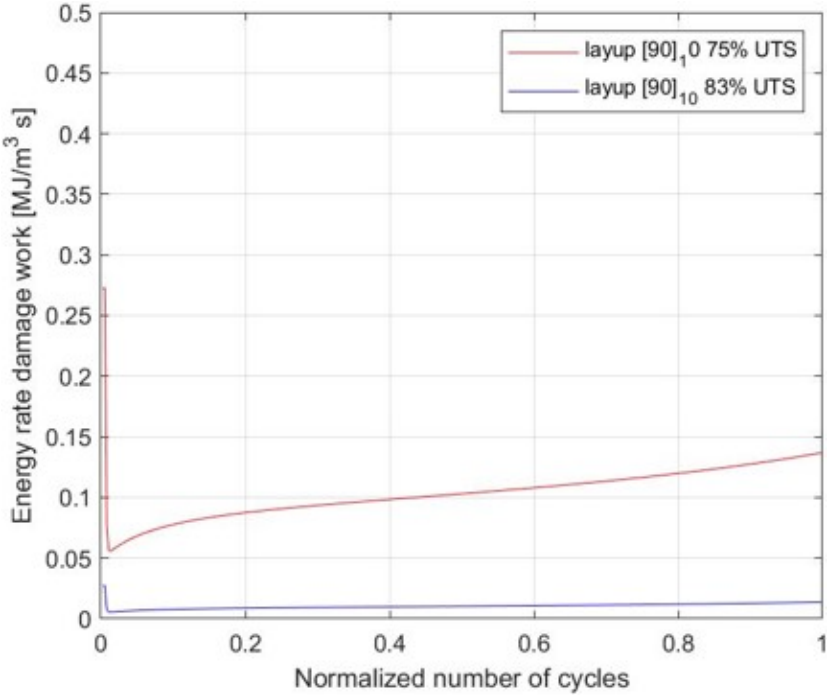


### 6.2.4 Huang's data

The idea of validating the model and then applying it to Huang's large collection of material data does not bring to results. Numerous parameters that require particular tests are missing. And a comparison with other CFRP laminates is not easy because the stacking sequence makes an important difference. The valuable aspect of Huang's data is that damage parameters are collected at numerous numbers of cycles and at multiple loading stresses. That is why, if the material properties are fulfilled with the missing values, that kind data collection are a very important resource in this field.

# 7 Conclusion

Advanced research in the composites field is aiming at a complete description and understanding of the damage phenomena and their possible effects by many points of view. In this case, damage evolution is monitored in order to quantify fatigue limit and fatigue-related mechanisms.

The goal of this work was to associate self-heating to damage evolution in CFRP laminates. A new proposed model, based on two previous solid models is now set up. Since it proposes a way to separate the energy sources, it can be the useful to uncouple degradation mechanisms. The RVE numerical model is a powerful tool to operate micro-scale analysis. For the moment, there is no other way than numerical simulation to investigate mechanical behavior at this scale. In addition, the composite can be considered effectively as a two phase system.

Early results are meaningful because they quantify energies. Accuracy of the values is not guaranteed for the moment because it needs a rigorous and complete database of material properties. The three models presented are limited in different ways. Huang's is lacking a analytical description of some aspects, Mahmoudi's and this work's models are lacking a complete set of measurements of specific mechanical properties.

Future developments can be:

- Implementation of Cohesive Zone Model (CZM) that allows to consider debonding and crack propagation in the numerical model
- Prediction of fatigue behavior multidirectional laminate through the definition of a constitutive model
- More data about materials, that means not only a more complete set of data on CFRP but to extend these models to GFRP, sandwiches, short fibre reinfroced composites...
- Analyze the cases of pre-damaged components or of specimens with prefabricated holes

# References


[1] T. Boulanger. "Calorimetric analysis of dissipative and thermoelastic effects associated with the fatigue behavior of steels". In: *International Journal of Fatigue* 26 (2004), pp. 221–229. ISSN: 01421123. DOI: \url{10.1016/S0142-1123(03)00171-3}.

[2] C. T. Sun and R. S. Vaidya. "Prediction of composite properties from a representative volume element". In: *Composites Science and Technology* 56 (1996), pp. 171–179.

[3] André Chrysochoos and Hervé Louche. "An infrared image processing to analyse the calorific effects accompanying strain localisation". In: *International Journal of Engineering Science* 38.16 (2000), pp. 1759–1788. ISSN: 00207225. DOI: \url{10.1016/S0020-7225(00)00002-1}.

[4] Willis J.R. Drugan W.J. "A micromechanics-based nonlocal constitutive equation and estimates of representative volume element size for elastic composites". In: *Mech. Phys. Solids* 44.4 (1995), pp. 197–524.

[5] Ashby M. F. *Materials Selection in Mechanical Design*. fourth edi. 2019.

[6] J. Huang. "Rapid Determination of Fatigue Behaviour for Carbon Fiber Reinforced Polymer Laminates Based on Thermodynamic Phenomena Observed by IR Thermography". PhD thesis. Université de Toulouse, 2019.

[7] J. Huang et al. "A new model for fatigue life prediction based on infrared thermography and degradation process for CFRP composite laminates". In: *International Journal of Fatigue* 120 (2019), pp. 87–95. ISSN: 01421123. DOI: \url{10.1016/j.ijfatigue.2018.11.002}.

[8] Jia Huang et al. "Investigation of self-heating and life prediction in CFRP laminates under cyclic shear loading condition based on the infrared thermographic data". In: *Engineering Fracture Mechanics* 229 (2020), pp. 1–14. ISSN: 00137944. DOI: \url{10.1016/j.engfracmech.2020.106971}.

[9] Jia Huang et al. “Rapid evaluation of fatigue limit on thermographic data analysis”. In: *International Journal of Fatigue* 104 (2017), pp. 293–301. ISSN: 01421123. DOI: \url{10.1016/j.ijfatigue.2017.07.029}.

[10] Sadik L. “Development of an ABAQUS plugin for periodic RVE homogenisation”. In: *Engineering with Computers* 35 (2018), pp. 567–577.

[11] Risitano A. La Rosa G. “Thermographic methodology for rapid determination of the fatigue limit of materials and mechanical components”. In: *International Journal of Fatigue* 22 (2000), p. 6573.

[12] Fard M. “Nonlinear Inelastic Mechanical Behavior Of Epoxy Resin Polymeric Materials”. PhD thesis. Arizona State University, 2011.

[13] Ali Mahmoudi and Bijan Mohammadi. “Theoretical-experimental investigation of temperature evolution in laminated composites due to fatigue loading”. In: *Composite Structures* 225 (2019), pp. 1–10. ISSN: 02638223. DOI: \url{10.1016/j.compstruct.2019.110972}.

[14] Marco Cattaneo. “Modellazione della resistenza post-impatto di laminati in composito”. PhD thesis. Politecnico di Milano, 2009.

[15] Marino Quaresimin. “Un approccio innovativo alla progettazione a fatica di strutture in materiale composito avanzato”. In: *Analisi e Calcolo* 85 (2020), pp. 1–11.

[16] Bijan Mohammadi, Babak Fazlali, and Davood Salimi-Majd. “Development of a continuum damage model for fatigue life prediction of laminated composites”. In: *Composites Part A: Applied Science and Manufacturing* 93 (2017), pp. 163–176. ISSN: 1359835X. DOI: \url{10.1016/j.compositesa.2016.11.021}.

[17] P. Ladeveze and E. Le Dantec. “Damage modelling of the elementary ply for laminated composites”. In: *Composites Science and Technology* 43 (1992), pp. 257–267.

[18] Liu Y. Peng. T. “In-situ fatigue prognosis for composite laminates based on stiffness degradation”. In: *Composite Structures* (2015).

[19] Zappalorto M. Ricotta M. *Introduzione ai materiali compositi*. Corso di Costruzione di Macchine 2. 2019.

[20] Varna J. Talreja R. "Modeling damage, fatigue and failure of composite materials". In: (2015).